Reviewed Preprint
v1 • September 16, 2026
Not revised

For correspondence:
Ingrid.winkler@mater.uq.edu.au
i.vetter@uq.edu.au

Competing interests: No competing interests declared

Funding: See page 24

Reviewing editor: Florent Ginhoux, Singapore Immunology Network, Singapore

E-Selectin Orchestrates IL-1β–Dependent Neuroinflammation via NLRP3 in Vincristine-Induced Neuropathy

Hana Starobova[a], Ammar Alshammari[a], Nikhil Nageshwar Inturi[b], Nicolette Tay[c], Svetlana Shatunova[a,d], Ali Lam[a], Quan Nguyen[a], Marisol Mancilla Moreno[b], Diana Tavares Ferreira[b], Federico Iseppon[e], Virginia Rodriguez-Menendez[e], Cristina Meregalli[e], Brittany Hill[a], Larissa Labzin[a], Simranpreet Kaur[d], Darren L Brown[a], Guido Cavaletti[e], Theodore Price[b], Avril Robertson[a,f], Allison Pettit[d], Jennifer L Stow[a], Ingrid G Winkler[d] ✉, Irina Vetter[a,c] ✉

[a]Institute for Molecular Bioscience, The University of Queensland, St Lucia, Australia • [b]Department of Neuroscience and Center for Advanced Pain Studies, University of Texas at Dallas, Richardson, United States • [c]School of Pharmacy and Pharmaceutical Sciences, The University of Queensland, Woolloongabba, Australia • [d]Mater Research Institute-The University of Queensland, Translational Research Institute, Woolloongabba, Australia • [e]Experimental Neurology Unit, School of Medicine and Surgery, University of Milano-Bicocca, Monza, Italy • [f]School of Chemistry and Molecular Biosciences, The University of Queensland, St Lucia, Australia

eLife Assessment

This paper provides a **useful** assessment of the role of macrophages in the development of functional paw withdrawal, which is a feature in the mouse model of vincristine-induced peripheral neuropathy (VIND). The authors suggest a role for E-selectin as a critical molecule promoting VIPN, acting via immune cell recruitment and inflammasome-mediated signalling; however, their data on NLRP3 inflammasome activation in vivo remains somewhat **incomplete**. This study will be of interest for immunologists.

https://doi.org/10.7554/eLife.111950.1.sa2

Abstract

Vincristine-induced peripheral neuropathy (VIPN) is a frequent and dose-limiting complication of cancer therapy, yet the upstream mechanisms coupling vascular activation to neuroinflammation remain poorly defined. Here we identify E-selectin as a critical orchestrator of vincristine-induced neuropathy. Systematic interrogation of endothelial adhesion molecules in a murine model of VIPN revealed that blockade of E-selectin, but not ICAM-1, PECAM-1 or P-selectin, completely prevented mechanical hypersensitivity and markedly reduced F4/80$^+$ immune cell accumulation in dorsal root ganglia and peripheral nerves. Genetic deletion of E-selectin conferred equivalent protection, despite the absence of structural loss of intraepidermal or myelinated fibres, indicating a predominantly functional neuroimmune pathology. Spatial transcriptomics demonstrated that vincristine induces a conserved stress and neuroinflammation-associated transcriptional programme in dorsal root ganglia, with immune and stromal populations acting as dominant signalling hubs. Genetic or pharmacological perturbation of E-selectin did not abolish injury-associated pathways but redistributed cell–cell communication networks, reducing immune-cell dominance and reshaping interferon and metabolic signalling states without inducing *Sele* expression. Mechanistically, E-selectin exerted non-canonical effects beyond endothelial adhesion. Local E-selectin administration was sufficient to induce macrophage-dependent mechanical hypersensitivity that was abolished in Fut4/7-deficient mice and following phagocyte depletion. In

macrophages, E-selectin enhanced vincristine-driven NF-κB activation, NLRP3 inflammasome assembly and IL-1β release. Together, these findings position E-selectin as an upstream regulator of IL-1β–dependent neuroinflammation in VIPN and identify selective targeting of E-selectin–mediated immune–neuron interactions as a therapeutic strategy for chemotherapy-induced neuropathy.

Introduction

Vincristine is a chemotherapeutic agent widely used in the treatment of paediatric and adult malignancies, including acute lymphoblastic leukaemia, Hodgkin's lymphoma, and neuroblastoma[1–3]. However, its clinical utility is frequently constrained by vincristine-induced peripheral neuropathy (VIPN), a dose-limiting and often irreversible adverse condition that affects up to 90% of paediatric patients and a substantial proportion of adults[4]. VIPN presents with a spectrum of sensory, motor, and autonomic disturbances that significantly impair quality of life and long-term functional outcomes in cancer survivors[5,6].

Although the underlying mechanisms of VIPN remain poorly understood, it is thought to involve microtubule disruption, impaired axonal transport, axonal degeneration, and mitochondrial dysfunction (reviewed in[6]). Recent studies have implicated neuroinflammation as a central driver of VIPN pathology[7–9]. Specifically, monocyte infiltration into dorsal root ganglia (DRG) and peripheral nerves initiates a cascade of immune activation, including the assembly of the NLRP3 inflammasome and release of pro-inflammatory cytokines such as interleukin-1β (IL-1β), a critical mediator of inflammatory pain[8,10–12]. Relevant to the clinic, inhibition of the NLRP3 inflammasome using MCC950, a selective NLRP3 inhibitor, alleviates vincristine-induced sensory and motor neuropathy in ALL-19 tumour-bearing NSG mice treated with a combination of vincristine, L-asparaginase, and dexamethasone[13]. However, while NLRP3-dependent inflammation has emerged as a key effector of vincristine neurotoxicity, the upstream signals that govern immune cell recruitment to peripheral nerves remain poorly defined.

Vincristine is known to upregulate the expression of intercellular adhesion molecule-1 (ICAM-1) and vascular cell adhesion molecule-1 (VCAM-1)[7], and it is plausible that enhanced adhesive properties of endothelial cells are critical drivers contributing to the infiltration of immune cells into neuronal tissue. However, the functional contribution of different families of adhesion molecules – including cell adhesion molecules and selectins – to the development of vincristine-induced neuropathy has not been systematically assessed. To address this gap, we investigated the contributions of VCAM-1, ICAM-1, PECAM-1, P-selectin and E-selectin to vincristine-induced mechanical hypersensitivity and neuronal immune cell infiltration.

Using a murine model of VIPN, we identify E-selectin as a critical driver of vincristine-induced peripheral neuropathy (VIPN). Pretreatment with an E-selectin–blocking antibody provided complete protection against vincristine-induced mechanical hypersensitivity, highlighting its essential role in neuropathy development. Moreover, E-selectin inhibition or genetic deletion conferred neuroprotection on transcriptional level in the dorsal root ganglia. Importantly, our findings also uncover a non-canonical signalling role of E-selectin in VIPN, where, in addition to immune cell infiltration, it promotes neuroinflammation by enhancing NF-κB activation and amplifying IL-1β release through the NLRP3 inflammasome.

Materials and methods

Animals, in vivo experiments and ethical approvals

Behavioural and *in vivo* experiments were performed using 8–10-week-old C57BL/6J, E-selectin knockout (*Sele*$^{-/-}$), fucosyltransferase 4/7 double knockout (*Fut4/7*$^{-/-}$), and ASC–citrine reporter mice. Mice were group-housed (3–5 per cage) under a 12 h light/dark cycle with ad libitum food and water. All procedures were approved by the University of Queensland Animal Ethics Committee and conducted in accordance with the Animal Care and Protection Regulation (Qld, 2012), the Australian Code for the Care and Use of Animals for Scientific Purposes (2013), and IASP

guidelines. Animals were acclimatised prior to testing, randomly assigned to treatment groups, and behavioural assessments were performed by blinded observers. Vincristine sulphate (Pfizer) was diluted in sterile phosphate-buffered saline (PBS) and administered intraperitoneally (i.p.) at 0.5 mg/kg (10 µl/g), as previously described[8]. Blocking antibodies against E-selectin, VCAM-1, ICAM-1, PECAM-1 (Bio X Cell), or P-selectin (BioLegend), or matching isotype controls (10 mg/kg; 10 µl/g) as well as anakinra (100 mg/kg, Sobi) were administered prior to vincristine administration. For intraplantar injections, recombinant mouse E-selectin (600 ng/injection; R&D Systems), human IgG isotype control (600 ng/injection; Invitrogen) or 1000 BMDMs were diluted in sterile PBS and injected intraplantar (i.pl.; 20 µl/paw) into the right hind paw of C57BL/6J or *Fut4/7*$^{-/-}$ mice under 2% isoflurane anaesthesia. Mechanical and thermal sensitivity of the hind paws was assessed using electronic von Frey and MouseMet thermal apparatuses (MouseMet; Topcat Metrology) as previously described [20]. To deplete phagocytic cells, mice received intraperitoneal (i.p.) injections of liposome-encapsulated clodronate (10 µl/g of 5 mg/mL; Liposoma) or control liposome-encapsulated PBS as described previously[8].

Quantification of cytokine release and ASC speck formation in BMDMs

Murine (C57BL6/J or ASC-citrine) bone marrow-derived macrophages (BMDMs) were isolated and cultured as previously described[14,15]. Cytokine and chemokine release was quantified following adhesion of BMDMs to plates coated with recombinant mouse E-selectin (5 µg/mL; R&D Systems), recombinant mouse P-selectin (5 µg/mL; R&D Systems), recombinant human IgG isotype control (5 µg/mL; Invitrogen), or Tris-buffered saline as a control by LEGENDplex^{TM} Mouse Macrophage/Microglia Panel (BioLegend) according to the manufacturer's protocol. Readouts from samples were obtained using a flow cytometer (Beckman Coulter CytoFLEX-S). Data were analysed using the Data Analysis Software Suite by BioLegend. The concentration of interleukin-1 beta (IL-1β) from ASC-Citrine reporter BMDMs was quantified using or ELISA kit (R&D Systems) according to the manufacturer's protocol. For ASC speck quantification, live-cell imaging was performed every 10 min for up to 220 min using a Nikon Ti-E inverted microscope with a Hamamatsu Flash 4.0 sCMOS camera. Supernatants were collected at the end and analysed for IL-1β by ELISA.

Quantification of DRG neuron BMDM adhesion to E-selectin

Dorsal root ganglia (DRGs) were isolated from 8-week-old male C57BL/6 mice as previously described [14,15,17,18]. Dissociated DRG neurons or BMDMs were seeded into 96-well plates pre-coated with recombinant mouse E-selectin, human IgG isotype control, or Tris-buffered saline (5 µg/mL; 24 h at 4°C). Cell suspensions were added and incubated at 4°C for 1 h to allow adhesion. Non-adherent cells were removed by washing three times with fresh DMEM-high glucose (40 µL/well). Adherent cells were counted under a light microscope by a blinded observer.

Nf-κB p65 Transcription Factor Assay

NF-κB activation was assessed using the NFκB p65 Transcription Factor Assay Kit (Abcam) following the manufacturer's instructions. Nuclear proteins were extracted from BMDMs 30 min post-treatment using the Abcam Nuclear Extraction Kit. Protein concentrations were measured via Nanodrop, and 20 µL of nuclear extract per sample was analysed in duplicate. Activated NF-κB p65 binding to DNA was detected using a specific antibody, HRP-conjugated secondary antibody, and a colorimetric readout at 450 nm. Absorbance was measured using a Tecan microplate reader, and data were analysed to compare NF-κB activity between conditions.

Immunohistochemistry and quantification of Intraepidermal Nerve Fibre (IENF) density

Dorsal root ganglia and sciatic nerves were collected 25 h post vincristine or vehicle injection, fixed in 10% neutral-buffered formalin (NBF), and embedded in paraffin as previously described[19]. Briefly, Paraffin sections (5 µm) were deparaffinised, rehydrated, and antigen-

retrieved with Proteinase K. After blocking with Background Sniper (BioCare Medical), sections were incubated with rat anti-mouse F4/80 (1:350; Novus Bio) for 2 h, followed by biotinylated secondary antibody, ABC amplification (Agilent Dako), and DAB detection. Nuclei were counterstained with haematoxylin. Isotype control (rat IgG2b; BioLegend) was used to confirm specificity. Slides were scanned (Olympus) and F4/80+ area quantified using Visiopharm by a blinded observer to assess macrophage infiltration across treatment groups. For quantification of IENF density, vincristine (0.5 mg.kg. i.p.; Pfizer) was injected 5 times a week for 4 weeks. 1 week after the final vincristine injection, plantar hind paw skin was collected, postfixed in 4% paraformaldehyde for 24 h at 4 °C, cryoprotected in 30% sucrose o/n, embedded in OCT (TissueTEK) and snap frozen using dry ice [22]. Tissue was sectioned into three non-consecutive 50 µm sections per animal (n = 4 animals per group) and stained using rabbit anti-PGP9.5 primary antibody (1:500; Dako, Z5116) followed by Alexa Fluor 555–goat anti-rabbit secondary antibody (1:1000; Invitrogen, A-21428) [22]. Sections were coverslipped with DAPI-containing mounting media (Fluoroshield, Sigma Aldrich, F6057). Images were acquired using a spinning-disc confocal microscope (Nikon Ti2/Andor Dragonfly). Image analysis was performed in FIJI (ImageJ). Intraepidermal nerve fibre density was expressed as the percentage of PGP9.5-positive area relative to total epidermal area.

Spatial transcriptomics

Eight-week-old male C57BL/6J mice were treated with either saline or vincristine (0.5 mg/kg, i.p.) once. Additional groups included C57BL/6J mice pre-treated with an E-selectin–blocking antibody (Bio X Cell, 200 µg/mouse, i.p. at two time points (-24h, -1h) prior to vincristine), and E-selectin knockout (*Sele*$^{-/-}$) mice treated once with vincristine (0.5 mg/kg, i.p.). Dorsal root ganglia (DRG) were collected 24h post vincristine treatment under RNase-free conditions and immediately embedded in chilled OCT compound (Tissue-Tek, Sakura, Japan), then flash-frozen in pre-cooled isopentane to preserve tissue morphology. The study included DRGs from lumbar level L3-L6 (both sides) from 3 mice per treatment condition. A total of 15 DRGs per condition were embedded in one OCT block, positioned on a uniform embedding plane for consistent sectioning. Blocks were stored at –80 °C until further processing. Cryosections were dried at 37 °C for 1 min, fixed in 100% methanol at –20 °C for 30 min, and stained with Mayer's haematoxylin (5 min) and eosin (2 min). Slides were mounted in 85% glycerol for imaging on a Zeiss Axio Z1 slide scanner. Library preparation followed the Visium Spatial Gene Expression User Guide (CG000239 Rev C, 10x Genomics). Sequencing was performed using an Illumina NextSeq 500 with the following read structure: Read1 – 28 bp, Index1 – 10 bp, Index2 – 10 bp, Read2 – 120 bp. Raw BCL files were processed using bcl2fastq (v2.7.0), and reads were aligned to the mouse reference genome using Space Ranger (v1.3.0, 10x Genomics).

Pseudo-bulk generation from Visium data and differential expression analysis

To obtain biologically independent replicates, Visium barcodes belonging to the same animal were summed to create one pseudo-bulk count matrix per animal. Aggregating at the animal level minimizes within-animal sampling noise and ensures that statistical inference pertains to variation across animals rather than across individual barcodes. Raw gene counts were analyzed in DESeq2 (Love et al., 2014). Size factors were estimated with the median-ratio method (each gene count divided by a barcode-specific factor derived from the geometric mean across samples), after which a batch term was included in the design formula to correct for sequencing batch effects (design = ~ batch + condition). DESeq2 fits a negative binomial generalized linear model and applies Wald statistics followed by Benjamini-Hochberg correction to identify differentially expressed genes. Log_2 fold-changes were shrunken with "ashr" (Stephens, 2017), improving effect-size ranking for low-count genes. Genes meeting p-adjusted $P \leq 0.05$ and $\log_2 FC \geq 0.585$(FC of 1.5) were reported as differentially expressed.

Spatial Transcriptomics Deconvolution with SPOTlight

Seeded non-negative matrix factorization (NMF) regression-based deconvolution was performed using the **SPOTlight** package (1.8.0) (Elosua-Bayes et al., 2021). Cell type proportions were inferred in the spatial transcriptomics dataset using a reference single-cell RNA-seq dataset containing previously annotated cell populations (Bhuiyan et al., 2024). Gene expression and metadata were extracted from the spatial transcriptomics data to construct a SpatialExperiment object. SPOTlight was then used to generate a deconvolution matrix based on the marker gene profiles from the reference single-cell clusters. Topic profiles representative of each cell type was projected onto spatial transcriptomic spots to estimate cellular composition.

Morphometrical evaluation of nerves

C57BL/6J or *Sele*$^{-/-}$ animals were treated with vincristine (0.5 mg/kg; i.p.; Pfizer) 5 times a week for 4 weeks as described previously 8. In week 5, animals were culled using CO_2 euthanasia and caudal nerves were collected from 3 animals/groups and fixed by immersion with 2% Glutaraldehyde in phosphate buffer solution (0.12M), post-fixed in 1% OsO4, and embedded in epoxy resin to be ready for morphometric examination, according to previously reported protocols [23,24]. 1.5-µm–thick semi-thin sections of the resin embedded nerves out of 3 animals/group were then cut and stained with methylene blue. Images were acquired with a Nexscope Ne920 AUTO light microscope using a 60X magnification objective. (TiEsseLab Srl, Milano, Italy). The acquired images were then analysed using Image Pro-Plus software, a computer-assisted image analyser (Media Cybernetics). The density (fibres/mm^2) and the axonal diameters of myelinated fibres (used to calculate the frequency distribution histograms) were measured in randomly selected sections again according to previously reported methods[23,24].

Data and statistical analyses

Data (except transcriptomic analyses) were analysed using GraphPad Prism v10. Behavioural data are presented as mean ± SEM, with a minimum of six animals per group ($n \geq 6$). Statistical significance as indicated in figures was set at adjusted $P < 0.05$.

Results

Inhibition of E-selectin and VCAM-1 mitigates vincristine-induced hypersensitivity and F4/80$^+$ immune cell accumulation in neuronal tissue

Several studies have reported that the development of vincristine-induced peripheral neuropathy (VIPN) is associated with an increased presence of F4/80$^+$ cells in the dorsal root ganglia (DRGs) and peripheral nerves[7,8,25,26]. This accumulation is likely driven by the infiltration of CX3CR1$^+$ monocytes into peripheral nerves[7]. Vincristine appears to facilitate this infiltration by enhancing the adhesive properties of endothelial cells, including through upregulating the expression of intercellular adhesion molecule-1 (ICAM-1) and vascular cell adhesion molecule-1 (VCAM-1)[7]. However, the role of other endothelial adhesion molecules, particularly selectins, in the infiltration of immune cells remains unclear, as is the functional contribution of these processes to the development of VIPN.

To investigate these questions, we administered blocking antibodies against E-selectin (E-sel Ab), P-selectin (P-sel Ab), VCAM-1 (VCAM1 Ab), ICAM-1 (ICAM1 Ab), and PECAM-1 (PECAM1 Ab) to vincristine-treated C57BL6/J mice and quantified both the number of F4/80-positive cells in DRGs and sciatic nerve, as well as mechanical hypersensitivity that arises as a result of vincristine treatment.

Consistent with previous studies reporting up-regulation of VCAM-1 following vincristine treatment, inhibition of VCAM-1 significantly alleviated vincristine-induced mechanical hypersensitivity at 5 h and 24 h post vincristine administration (Fig. 1A; Supplementary Table 1)

and also significantly reduced F4/80$^+$ staining, indicative of monocyte/macrophage infiltration, in both DRGs and sciatic nerves (Fig. 1B, Fig. S2, Supplementary Table 2). In contrast, inhibition of ICAM-1 did not significantly alleviate vincristine-induced hypersensitivity (Fig. 1C, Supplementary Table 1), nor prevented infiltration of F4/80$^+$ cells in DRGs or sciatic nerves (Fig. 1D; Fig. S2 and Supplementary Table 2). Additionally, PECAM-1 inhibition only partially alleviated vincristine-induced hypersensitivity (Fig. 1E, Supplementary Table 1) and did not prevented infiltration of F4/80$^+$ cells in DRGs or sciatic nerves (Fig 1F, Fig. S2 and Supplementary Table 2). Similar results were also observed following treatment with a P-selectin blocking antibody, which partially improved the vincristine-induced decrease in paw withdrawal threshold at 5 hours but not at 24 h compared to the IgG2a (Fig. 1G; Supplementary Table 1), and had no significant effect on the number of F4/80$^+$ cells in the DRGs or sciatic nerve (Fig. 1H; Fig. S2 and Supplementary Table 2).

Interestingly, inhibition of E-selectin prior to vincristine administration significantly (compared to the IgG2b) and completely prevented development of vincristine-induced mechanical hypersensitivity (Fig. 1J; Supplementary Table 1), and also significantly reduced the number of F4/80$^+$ cells in both the DRGs and sciatic nerves (Fig. 1K; Fig. S2 and Supplementary Table 2).

Vincristine-induced mechanical hypersensitivity is attenuated in *Sele*$^{-/-}$ mice

Although E-selectin has been highlighted by a number of studies as a putative biomarker for pain, it has not previously been implicated as an analgesic target in chemotherapy-induced neuropathy. We thus sought to further investigate the molecular mechanisms contributing to anti-allodynic effects of E-selectin inhibition, as well as the potential of E-selectin-targeting therapeutics for treatment or prevention of vincristine-induced neuropathy.

We first sought to confirm that the phenotype observed following inhibition of E-selectin signalling with blocking antibodies – decreased immune cell infiltration in neuronal tissues, and decreased vincristine-induced mechanical hypersensitivity – also occurs in E-selectin knockout (*Sele*$^{-/-}$) mice. Indeed, *Sele*$^{-/-}$ mice were fully protected from vincristine-induced mechanical hypersensitivity, whereas C57BL6/J (wt) mice exhibited a sustained decline in paw withdrawal thresholds (PWTs) (Fig. 2A; Supplementary Table 3). Furthermore, the accumulation of F4/80$^+$ immune cells was significantly reduced in both the dorsal root ganglia (Fig. 2B) and sciatic nerves (Fig. 2C) of *Sele*$^{-/-}$ mice compared to vincristine-treated C57BL6/J controls at 25 h post first vincristine administration (Fig. 2B-D; Supplementary Table 4). To determine whether E-selectin deletion confers structural neuroprotection during vincristine exposure, we next quantified intraepidermal nerve fibre density and myelinated fibre integrity by immunohistochemistry and electron microscopy. Notably, no significant differences were detected between saline- and vincristine-treated groups in either genotype. Intraepidermal fibre density in footpads was comparable across C57BL/6J and *Sele*$^{-/-}$ mice (Fig. 2D). Similarly, vincristine did not alter myelinated fibre density (representative images, Fig. 2F; quantification, Fig. 2G) or the relative frequency distribution of myelinated fibre calibres in caudal nerves (Fig. 2H). Together, these findings indicate that vincristine induces sustained mechanical hypersensitivity that is prevented in *Sele*$^{-/-}$ mice, without causing detectable structural loss of small or myelinated fibres.

Cell–cell communication roles are reprogrammed by E-selectin perturbation during vincristine treatment

Given the absence of detectable morphological neuronal damage in our vincristine model (Fig. 2E–H), we next employed spatial transcriptomics to identify molecular signatures of neuronal stress or injury and to define processes driving neuronal dysfunction in vincristine-induced peripheral neuropathy (VIPN). This approach also enabled us to determine whether genetic or pharmacological perturbation of E-selectin confers neuronal protection at the transcriptional level. Dorsal root ganglia (DRG) were collected following a single vincristine (0.5 mg kg^{-1}, i.p.) or

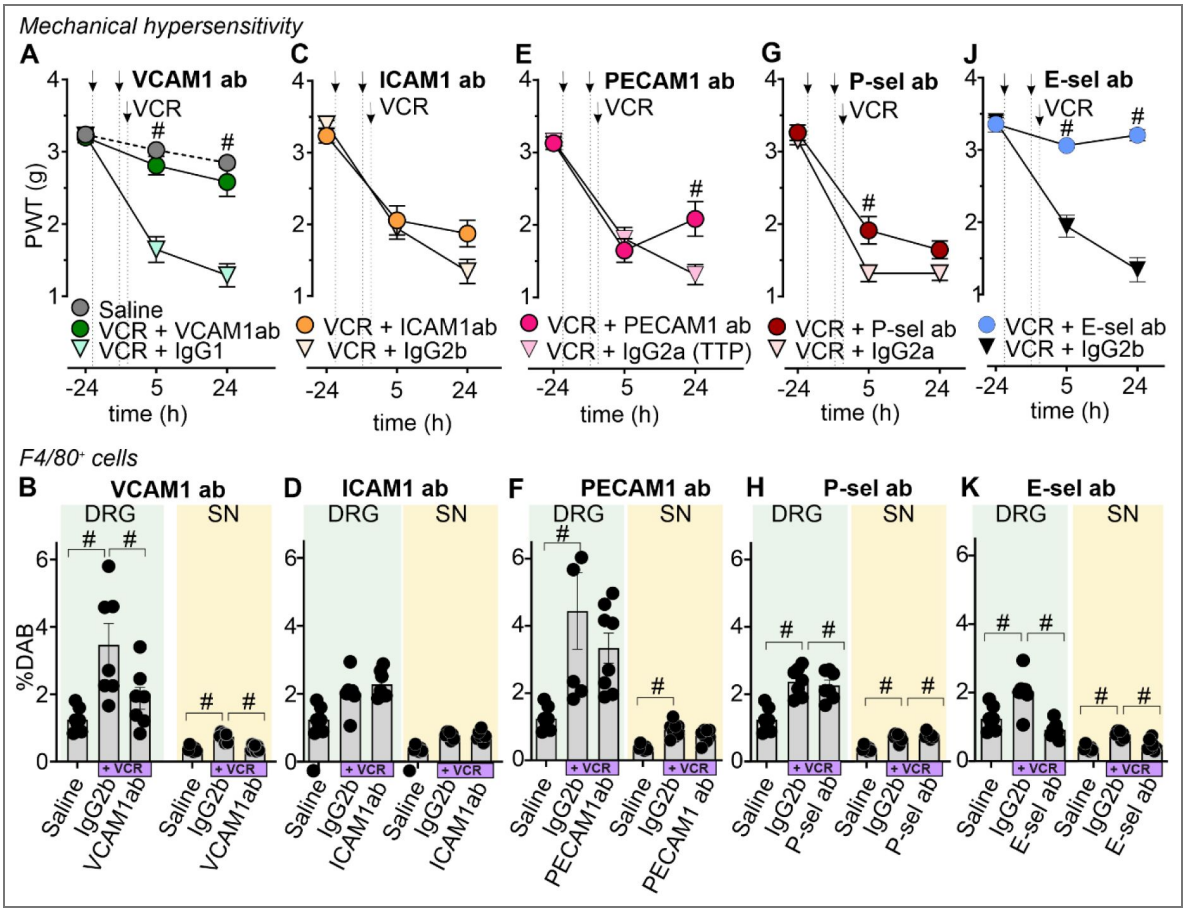

Fig. 1. Inhibition of E-selectin and VCAM-1, but not other adhesion molecules, attenuates vincristine-induced mechanical hypersensitivity and F4/80⁺ immune cell accumulation in the dorsal root ganglia (DRG) and sciatic nerves (SN).

The effect of blocking antibodies against VCAM-1 (VCAM1ab; **A, B**), ICAM-1 (ICAM1ab;**C,D**); PECAM-1 (**E,F**), P-selectin (P-sel ab; **G,H**) and E-selectin (E-sel ab; **J,K**) on vincristine-induced mechanical hypersensitivity (**A,C,E,G,J**; paw withdrawal threshold (g)) and the number of F4/80⁺ cell in dorsal root ganglia (DRG) and sciatic nerve (SN) (**B,D,F,H,K**; %DAB). Black arrows indicate injection (i.p.) of antibodies (10 mg/kg), isotype control antibodies (IgG2B, IgG1; (10 mg/kg)) and vincristine (0.5 mg/kg). Both VCAM-1 and E-selectin blocking antibodies alleviated vincristine-induced mechanical hypersensitivity (**A,J**) as well as the increase in F4/80⁺ cells in dorsal root ganglia (DRG) and sciatic nerve (SN) (**B,K**), while PECAM-1 and P-selectin blocking antibodies were partially effective (**E-H**) and ICAM-1 blocking antibody had not effect (**C,D**). Data are presented as mean ± SEM (n = 5–7 per group). Statistical significance (# $p < 0.05$) was determined using repeated-measures two-way ANOVA or one-way ANOVA with Šídák's multiple comparisons test.

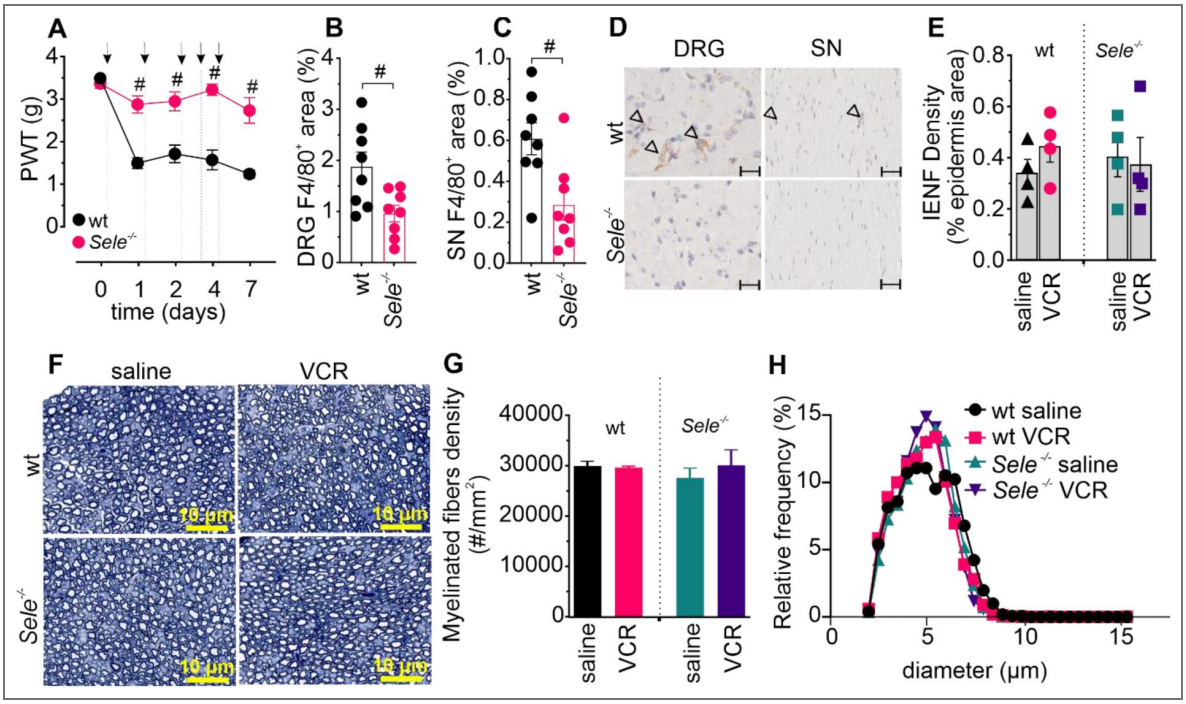

Fig. 2. Vincristine induces mechanical hypersensitivity and F4/80⁺ macrophage accumulation, but not peripheral nerve damage, that is attenuated in Sele⁻/⁻ mice.

(A) Sele⁻/⁻ mice were protected from vincristine-induced mechanical hypersensitivity compared to wt C57BL6/J controls. Mice received vincristine (VCR) for five consecutive days (black arrows), and mechanical hypersensitivity was assessed at baseline (0 h) and on days 1, 2, 4 and 7 post-treatment. **(B,C)** In contrast to wt C57BL6/J mice, Sele⁻/⁻ mice treated with vincristine were protected from F4/80⁺ cell accumulation in the dorsal root ganglia (DRG) and sciatic nerve (SN) 25 h after the first vincristine administration. **(D)** Representative images of F4/80⁺ immunoreactivity in DRG and SN from wt C57BL6/J and Sele⁻/⁻ mice. Arrowheads indicate F4/80⁺ areas. Scale bars, 20 µm (DRG) and 10 µm (SN). **(E-H)** Vincristine does not cause structural damage to peripheral nerve fibres. No significant differences in intraepidermal nerve fibre (IENF) density **(E)**, myelinated fibre density **(F,G)** or relative myelinated fibre size distribution in caudal nerves (H) were observed between saline and vincristine treatments in both wt C57BL6/J and Sele⁻/⁻ mice. **(F)** Representative images of myelinated fibres in caudal nerves of wt C57BL/6J and Sele⁻/⁻ mice treated with vincristine or saline. Scale Bar 10 µm. Statistical analyses were performed using repeated-measures two-way ANOVA with Sidak's multiple-comparison test **(A,H)** or two-tailed t-tests **(B–G)**. #: $P < 0.05$; n = 3–8 per group.

saline injection from C57BL6/J mice, *Sele*$^{-/-}$ mice, and C57BL6/J mice pre-treated with two doses of E-selectin–neutralising antibody, and analysed for gene expression changes and spatial distribution patterns.

First, we performed a pseudobulk analysis of differentially expressed genes (DEGs). Comparing saline-treated C57BL6/J mice to vincristine-treated C57BL6/J mice, we identified 33 upregulated and 44 downregulated genes (Supplementary Fig. S2A; Supplementary Table 5A). Among the most significantly upregulated genes were Map1b (microtubule associated protein 1B) and Hcn2 (hyperpolarisation activated cyclic nucleotide gated potassium and sodium channel 2). Additionally, the most significantly downregulated genes included genes of the haemoglobin family, the Hba-a2 (haemoglobin subunit alpha 2), Hba-a1 (haemoglobin subunit alpha 1) and Hbb-bs (haemoglobin subunit beta).

Enrichment (MsigDB) analysis of DEGs showed robust and conserved stress response in dorsal root ganglia characterised by enrichment of mTORC1 signalling, cholesterol and lipid homeostasis, and proteostasis pathways, including the unfolded protein response (UPR), together with activation of p53 and apoptosis modules (Supplementary Tables 6–7). At the gene level, this transcriptional backbone was accompanied by induction of injury- and excitability-associated transcripts (Supplementary Table 5A), including stress and remodelling markers (e.g. Jun, Map1b) and excitability-linked genes such as Hcn2, alongside downregulation of antigen-presentation genes (e.g. Cd74, H2-Aa, H2-Eb1).

Comparing vincristine-treated C57BL6/J mice to vincristine-treated *Sele*$^{-/-}$ mice, we identified 214 upregulated and 97 downregulated genes (Supplementary Fig. S2B; Supplementary Table 5B), while comparison between vincristine-treated C57BL6/J mice and C57BL6/J mice pre-treated with E-selectin antibody (Esel-ab) prior to vincristine revealed 151 upregulated and 34 downregulated genes (Supplementary Fig. S3C; Supplementary Table 5C). Among the most significantly upregulated genes in both comparisons were *Scand1* (encoding SCAN domain-containing protein 1) and *Hspb1* (encoding heat shock factor binding protein 1), both transcription factors potentially involved in modulating cellular stress responses. Among the downregulated genes in comparisons were *Bst2* (encoding tetherin) and *Ly6a* (encoding stem cell antigen-1), both of which play key roles in the regulation of immune responses. The complete lists of up- and downregulated genes for all conditions are provided in Supplementary Table 5. Enrichment analysis of DEGs revealed that perturbation of E-selectin signalling, either by genetic deletion or pharmacological blockade, was associated with prominent modulation of interferon α/γ response pathways, together with enrichment of hypoxia, epithelial–mesenchymal transition, and immune–vascular signalling programs (Supplementary Tables 8–11). Both *Sele*$^{-/-}$and Esel-ab conditions converged on a shared interferon-associated transcriptional module, including *Stat1*, *Stat2*, *Ifitm3*, *Ly6e* and *Bst2*, as well as an extracellular matrix component (*Col1a1*) indicating a conserved E-selectin–sensitive immune state under vincristine challenge. Notably, while the overall transcriptional profiles were overlapping, pharmacological E-selectin blockade exhibited a distinct metabolic signature, with additional enrichment of oxidative phosphorylation, reactive oxygen species, and unfolded protein response pathways (Supplementary Tables 10–11), consistent with altered bioenergetic and proteostatic adaptation relative to the knockout condition.

In our transcriptome, we did not detect increased expression of *Sele* mRNA following vincristine treatment in DRGs. To confirm that vincristine administration is not accompanied with increased E-selectin expression, we also quantified soluble E-selectin (sE-sel) protein in plasma following treatment with vincristine, which failed to detect significant changes in E-selectin expression at the protein level (Supplementary Fig. S3D). Similarly, *Sele* levels analysed using PCR, remained unchanged in the human endothelial cell line HUVEC following exposure to vincristine (Supplementary Fig. S3E).

Spotlight analysis identified several neuronal and non-neuronal subtypes within the specific treatment groups (Supplementary Fig. S3F). Therefore, we next assessed changes in specific cell type-mediated signalling using CellChat analysis to further understand how deletion or inhibition of E-selectin may mediate protection from mechanical hypersensitivity in our VIPN model (Fig. 3, Supplementary Fig. 4, Supplementary Table 12). CellChat analysis revealed a

communication network in which immune cells, fibroblasts, pericytes, and Schwann cells act as dominant senders across multiple injury-associated pathways following vincristine treatment (C57BL6/J (VCR); sSupplementary Table 12) including Spp1 (osteopontin), Galectin (β-galactoside–binding lectins), Sema3 (semaphorin 3), Kit (stem cell factor receptor), Nrg (neuregulin), Nt (neurotrophins), Nts (neurotensin) and Fgf (fibroblast growth factors) that collectively regulate inflammatory adhesion, immune modulation, axon guidance, growth factor activation, glial support, neuronal survival, pain signalling and tissue remodelling, while sensory neuron subtypes function primarily as receivers (Fig. 3A,C,E,G; Supplementary Fig. 4A–E). In particular, immune and support cell populations showed high sender and influencer scores for Spp1, Galectin and Sema3, indicating that these cells not only initiate signalling but also strongly shape network structure.

For Spp1 signalling, immune, fibroblast, Schwann cells and Pvalb neurons (interneurons) were the principal senders and influencers, expressing Spp1 (ligand), while nociceptive and peptidergic neurons (Calca^{+}Bmpr1b, Calca^{+}Smr2, Mrgpra3^{+}Trpv1, Ntrk3^high/+Ntrk2) acted as dominant receivers, expressing CD44 and integrin receptors (Itgav/Itgb1, Itgav/Itgb5) (Fig. 3A, B, Supplementary Table 12). Fibroblasts and Schwann cells additionally showed elevated mediator scores, consistent with their role in relaying immune-derived signals through the neurovascular niche.

Galectin signalling was driven by neuronal senders (Calca^{+}Bmpr1b, Calca^{+}Smr2, Mrgpra3^{+}Trpv1, Mgprd) expressing Lgals9, with immune, Schwann cell, fibroblast and some neuronal populations as primary receivers via CD44 and Ighm receptors (Fig. 3C, D, Supplementary Table 12). Ptn signalling was dominated by Calca^{+}Bmpr1b neurons, Pvalb interneurons and fibroblast as major sender via Ptn sending signals towards a mixed population (Fig. 3E, F, Supplementary Table 12). Sema3 signalling showed strong non-neuronal sender and influencer activity, with Sema3b/f/g ligands produced by immune cells, fibroblasts and Schwann cells, while Mrgpra3^{+}Trpv1 neurons served as the dominant receivers via Nrp2/Plxna2 and Nrp2/Plxna4 complexes (Fig. 3G,H, Supplementary Table 12). Collectively, this data suggests that vincristine establishes a network in which immune and stromal cells act as upstream signal initiators and network shapers, delivering injury-associated cues to neuronal targets.

In E-selectin-deficient animals treated with vincristine (Sele$^{-/-}$ (VCR)), CellChat analysis demonstrated a marked redistribution of communication roles rather than pathway loss (Fig. 3I–P; Supplementary Table 12, Supplementary Fig. 4F–J). For Spp1, compared to C57BL6/J (VCR), ligand expression in Sele$^{-/-}$ (VCR) was reduced in immune cells, fibroblasts and Schwann cell acting as senders, while neurons somewhat retained receiver capacity through CD44 and integrins, but with increased influencer coupling (Fig. 3I,J, Supplementary Table 12). Galectin signalling showed a reduction in almost all cell types, with Calca^{+}Smr2 dominating the signalling pathway (Fig. 3K,L, Supplementary Table 12). Ptn signalling in Sele$^{-/-}$ (VCR) showed decreased sender and mediator roles for immune cells and fibroblasts, while Schwann cell and pericytes signals increased, dominated by Ntrk3^high/+Ntrk2 neurons. Ptn signalling pathway was modulated via Ptprz1 ligand and syndecan receptors (Sdc1–4) (Fig. 3M,N, Supplementary Table 12). In Sema3, non-neuronal sender and influencer scores were reduced, and signalling was redistributed among non-neuronal populations (Fig. 3O,P, Supplementary Table 12).

Pharmacological blockade of E-selectin (C57BL/6J (Esel-ab + VCR)) produced a communication architecture that overlapped with, but extended beyond, the knockout condition (Supplementary Fig. 4K–S, Supplementary Table 12). In this setting, immune cells, fibroblasts and Schwann cells showed further reduction in sender and influencer roles across injury-associated pathways. Additionally, we observed a striking dysregulation of genes involved in inflammatory pathways in *Sele*$^{-/-}$ treated with vincristine (Supplementary Tables 8-9) suggesting that E-selectin may act as an upstream driver of neuroinflammation in VIPN, potentially by modulating inflammatory processes, such as interferon-related immune activation. To further investigate this, we performed gene expression plot of immune signalling associated genes in *Sele*$^{-/-}$ to determine cell populations that are primarily responsible for the shift in inflammation-associated genes (Fig. 3Q). Interferon-responsive transcripts, including *Stat1*, *Stat2*, *Ifitm3*, *Bst2*, *Ly6e* and *Isg15*, were

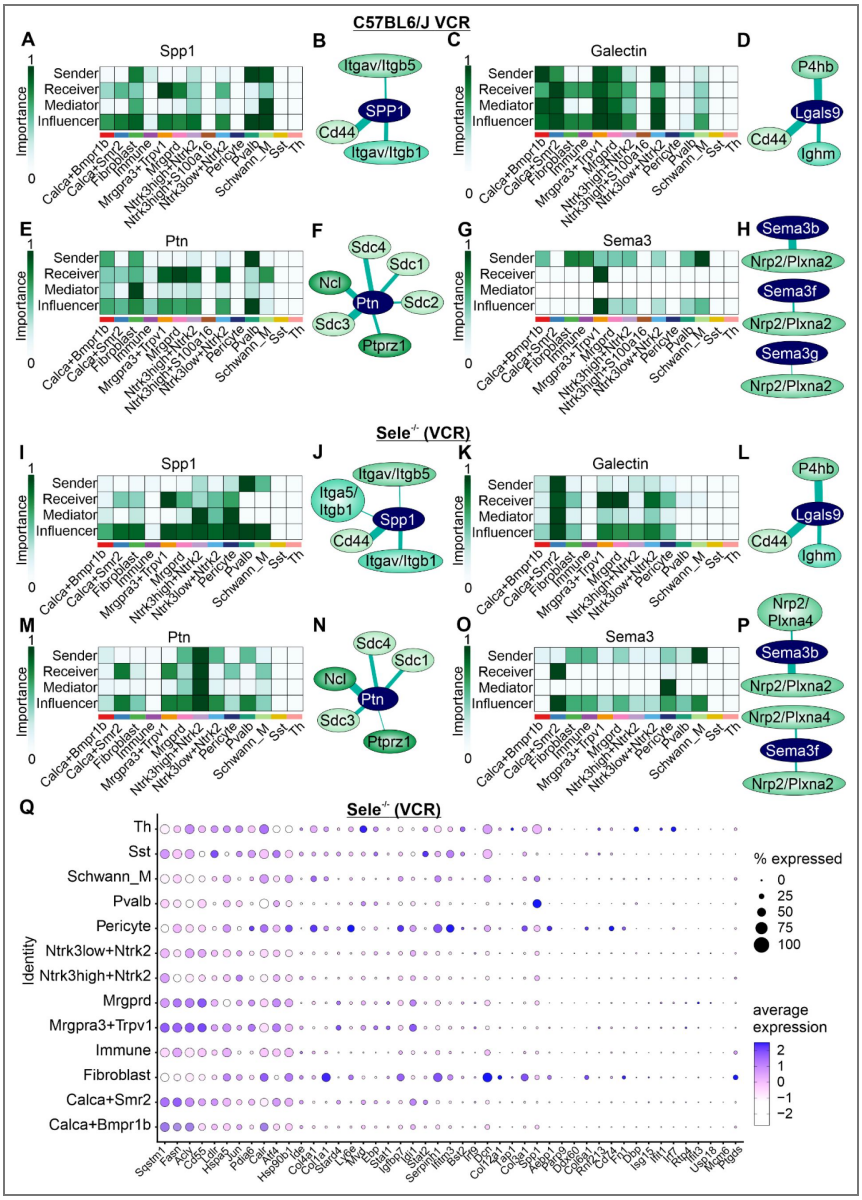

Fig. 3. Vincristine reshapes cell-cell communication in dorsal root ganglia through injury-associated signalling pathways.

CellChat analysis was used to infer ligand–receptor–mediated communication networks in dorsal root ganglia (DRG) following vincristine treatment, revealing pathway-specific sender, receiver, mediator and influencer roles across neuronal and non-neuronal populations. Heatmaps **(A,C,E,G,I,K,M,O)** show the relative importance of each cell type as senders, receivers, mediators or influencers, with darker green indicating greater contribution. Network schematics **(B,D,F,H,J,L,N,P)** depict dominant ligand–receptor interactions (thickness of the connector line depicts the relative contribution of the L-R pair). **(A-H)** Analysis of Spp1 **(A,B)**, galectin **(C,D)**, Ptn **(E,F)** and Sema3 **(G,H)** signalling in vincristine-treated C57BL6/J mice. (I–P) Corresponding analyses in Sele^{-}/$^{-}$ mice treated with vincristine demonstrate preservation of the same signalling pathways but redistribution of communication roles, with changed immune-cell, stromal and glial populations participation as senders, mediators and influencers across Spp1, galectin, Ptn and Sema3 pathways. **(Q)** Dot plot showing average expression (colour scale) and proportion of expressing cells (dot size) for immune pathway-associated genes across all annotated cell types in Sele^{-}/$^{-}$ (VCR) mice. VCR: vincristine; Sele^{-}/$^{-}$: E-selectin–deficient mice; DRG: dorsal root ganglion; Schwann_M: myelinating Schwann cells; Calca^{+}Bmpr1b and Calca^{+}Smr2: peptidergic sensory neuron subtypes expressing Calca with Bmpr1b or Smr2, respectively; Mrgprd: non-peptidergic sensory neurons; Mrgpra3^{+}Trpv1: nociceptive/pruriceptive neurons; Ntrk3^high/+Ntrk2 and Ntrk3^low/+Ntrk2: sensory neuron subsets defined by relative Ntrk3 and Ntrk2 expression; Pvalb: parvalbumin-expressing interneurons; Sst: somatostatin-expressing neurons; Th: tyrosine hydroxylase–expressing neurons; Immune: aggregated immune cell populations; Itgav/Itgb: integrin αV/β subunits; Nrp: neuropilin; Plxna: plexin A.

enriched predominantly within immune cell clusters (Fig. 3Q), defining a concentrated innate immune signalling module. Fibroblasts and pericytes displayed strong expression of extracellular matrix and remodelling genes (*Col1a1*, *Col3a1*, *Col4a1*, *Col12a1*, *Dcn*, *Fn1*), while Schwann cells co-expressed immune-responsive (*Ifitm3*, *Ly6e*) and matrix-associated (*Col4a1*, *Serpinh1*) transcripts, positioning them at the interface of immune–stromal signalling. In contrast, sensory neuron subtypes (*Calca*$^{+}$*Bmpr1b*, *Calca*$^{+}$*Smr2*, *Mrgpra3*$^{+}$*Trpv1*, *Mrgprd*, *Ntrk3*-defined populations) exhibited minimal interferon or extracellular matrix gene expression but retained stress-associated transcripts (*Jun*, *Atf4*, *Hspa5*).

In summary, under vincristine treatment, dorsal root ganglia exhibit a transcriptional and cell-cell communication profile marked by activation of stress, interferon, and immune–stromal signalling programs, with immune cells, fibroblasts, pericytes, and Schwann cells acting as dominant senders and influencers across multiple injury-associated pathways while sensory neurons function primarily as receivers. In contrast, genetic deletion or pharmacological blockade of E-selectin preserves these pathways but redistributes communication roles, reducing immune-cell dominance, altering interferon- and metabolism-associated gene expression, and increasing the involvement of stromal and glial populations in signal mediation.

E-selectin-induced mechanical hypersensitivity is mediated by immune cells

Spatial transcriptomic analyses indicated that E-selectin may influence vincristine-induced mechanical hypersensitivity through modulation of immune cell activity and inflammatory signalling, extending beyond its canonical role as an endothelial adhesion molecule. To directly assess this possibility, we administered recombinant E-selectin locally into the hind paw of C57BL6/J mice (intraplantar, i.pl.) and quantified mechanical paw withdrawal thresholds. This approach permitted investigation of the direct effects of E-selectin on peripheral immune or neuronal cells, bypassing the vascular endothelium and excluded confounding effects from endothelial adhesion.

Remarkably, i.pl. injection of E-selectin induced robust mechanical hypersensitivity, detectable as early as 1 hour post-injection and persisting at 4, 24, and 48 hours (Fig. 4A; Supplementary Table 13). In contrast, saline or IgG2b controls failed to induce hypersensitivity (Fig. 4A; Supplementary Table 13). Notably, E-selectin injection did not produce heat hyperalgesia (Fig. 4B). This mechanical hypersensitivity was accompanied by a significant increase in F4/80^{+} cell area in injected footpads compared to saline or IgG2b (Fig. 4C), with representative immunohistochemistry shown in Figure 4D.

To confirm ligand specificity, i.pl. E-selectin injection was repeated in Fut4/7$^{-/-}$ mice, which lack functional α(1,3)-fucosyltransferases required for the synthesis of E-selectin ligands[27]. Fut4/7$^{-/-}$ mice did not develop mechanical hypersensitivity following E-selectin injection (Fig. 4E), and their footpad F4/80^{+} area was significantly reduced compared to C57BL6/J-E-selectin treated animals and indistinguishable from IgG2b controls (Fig. 4F).

To define the cellular mediators of this hypersensitivity, adhesion assays were performed using dorsal root ganglia (DRG) neurons and bone marrow–derived macrophages (BMDMs) seeded onto E-selectin–coated surfaces. DRG adhesion was unaffected by E-selectin (Fig. 4G), suggesting little to no direct interaction between neurons and E-selectin. In contrast, BMDMs exhibited significantly increased adhesion to E-selectin compared to controls, which was abolished by E-selectin–blocking antibodies (Fig. 4H). These findings suggest that E-selectin primarily interacts with immune cells, such as macrophages, rather than neurons.

To further confirm the specific role of immune-mediated mechanisms in E-selectin–induced mechanical hypersensitivity, phagocytic cells were depleted with liposomal clodronate (CLD), with depletion confirmed in spleens (Fig. 4I). C57BL6/J mice pretreated with CLD or control liposomes (LIP) then received i.pl. injections of E-selectin, IgG2b, or saline (Fig. 4J). While LIP-pretreated mice developed sustained mechanical hypersensitivity following E-selectin injection, CLD-pretreated mice failed to develop hypersensitivity (Fig. 4J, Supplementary Table 14). No

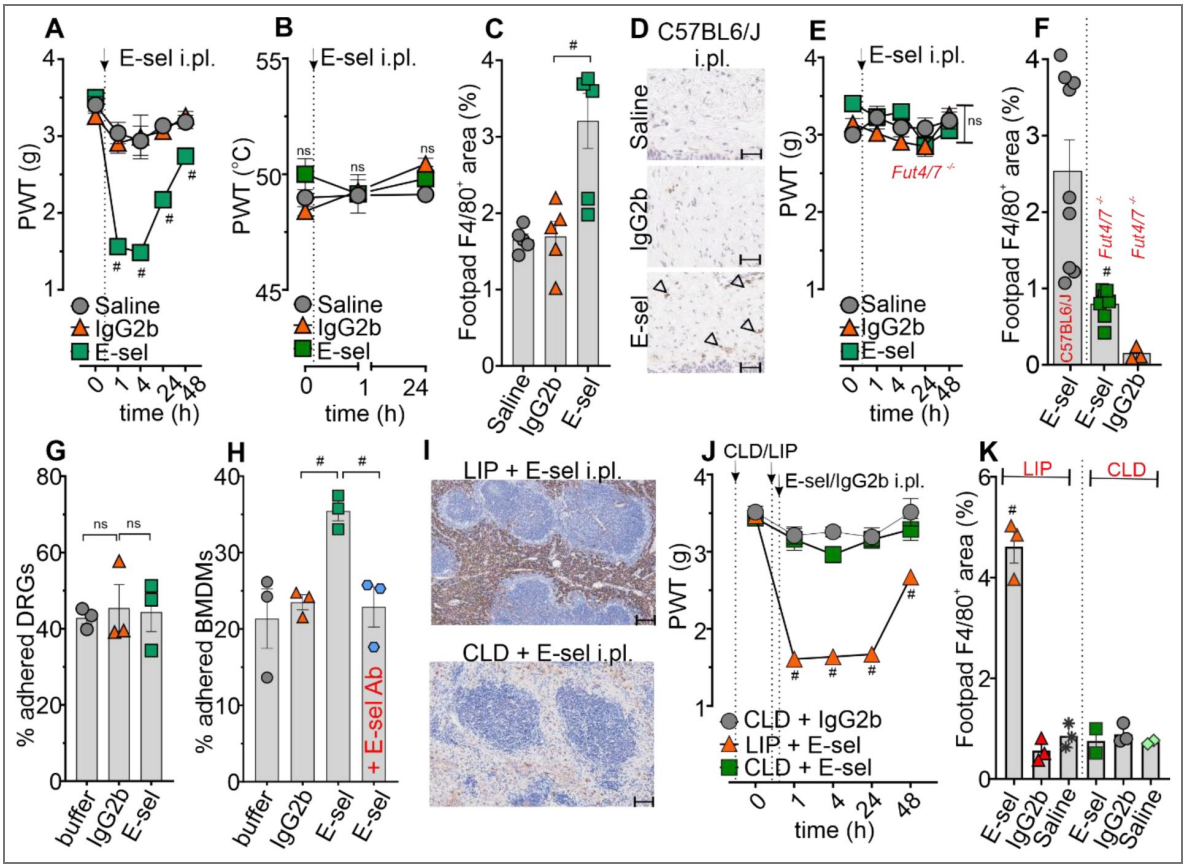

Figure 4. E-selectin-induced mechanical hypersensitivity is mediated by immune cells.

(A) Local intraplantar (i.pl.) injection of E-selectin – but not saline or IgG2b – into the hind paw of C57BL6/J mice induces significant mechanical hypersensitivity, **(B)** but not thermal hypersensitivity, and is **(C)** accompanied by an increase in F4/80$^+$ cells in the injected footpads. **(D)** Representative images of F4/80$^+$ cells in the E-selectin, IgG2b and saline-injected food pads. Scale bar = 10 µm. **(E)** Fut4/7$^{-/-}$ mice are protected from E-selectin-induced mechanical hypersensitivity and **(F)** the E-selectin-induced increase in F4/80$^+$ cell area. **(G–H)** Adhesion of dorsal root ganglion neurons (DRG) or bone marrow-derived macrophages (BMDMs) to E-selectin (E-sel), isotype control (IgG2b), or buffer. **(G)** E-selectin does not increase DRG neuron adhesion, but **(H)** significantly increases BMDM adhesion, which is significantly reduced by pre-treatment with an E-selectin–blocking antibody (E-sel Ab). **(I)** Representative immunohistochemical images of F4/80$^+$ cells in the spleens of C57BL6/J mice pretreated with clodronate (CLD) or liposome control (LIP) and injected i.pl. with E-sel, demonstrating effective depletion of F4/80$^+$ cells. Scale bar = 10 µm. **(J)** Pretreatment with liposomal clodronate (CLD) protects C57BL6/J mice from E-selectin-induced mechanical hypersensitivity. **(K)** CLD pretreatment also significantly reduces the increase in F4/80$^+$ cell area in the footpad following i.pl. E-selectin injection. Statistical significance (#: $P < 0.05$) was determined using one-way ANOVA for C, F, G, H (n=3-9) or repeated measures two-way ANOVA for A, B, E, J,K (n = 6-9).

hypersensitivity was observed in saline or IgG2b controls (Supplementary Fig. S4A). Consistent with this, CLD pretreatment significantly reduced F4/80$^+$ cell area in injected footpads (Fig. 4K), with representative images shown in Supplementary Fig. S4B.

E-selectin adhesion enhances interleukin-1β release in vincristine-treated BMDMs

We next investigated whether E-selectin adhesion alters vincristine-induced cytokine and chemokine release in BMDMs to determine whether the role of E-selectin in development of vincristine-induced neuropathy is restricted to its known canonical cell adhesion function. As expected, LPS + VCR treatment significantly increased (~40-fold) the secretion of interleukin-1β (IL-1β) in BMDMs (Fig. 5A). Interestingly, we also detected a significant increase of interleukin-18 (IL-18, Fig. 5B), interleukin-10 (IL-10, Fig. 5C), granulocyte colony-stimulating factor (G-CSF, Fig. 5D), interleukin-12 subunit p40 (IL-12p40, Fig. 5E), interleukin-6 (IL-6, Fig. 5F) and the chemokine C-X-C motif chemokine ligand 1 (CXCL1, Fig. 5G) (values of the cytokines in test and control conditions are shown in Supplementary Table 15). No significant changes were observed for tumour necrosis factor alpha (TNF-α), transforming growth factor beta 1 (TGF-β1), interleukin-23 (IL-23), interleukin-12 p70 heterodimer (IL-12p70), C-C motif chemokine ligand 17 (CCL17; also known as thymus and activation-regulated chemokine, TARC), or C-C motif chemokine ligand 22 (CCL22; also known as macrophage-derived chemokine, MDC) (Supplementary Table 15).

Interestingly, adhesion of BMDMs to E-selectin significantly enhanced the release of interleukin-1 beta (IL-1β) and interleukin-10 (IL-10), but not interleukin-18 (IL-18, Fig. 5H), granulocyte colony-stimulating factor (G-CSF, Fig. 5I), interleukin-12 subunit p40 (IL-12p40, Fig. 5J), interleukin-6 (IL-6, Fig. 5K), and C-X-C motif chemokine ligand 1 (CXCL1, Fig. 5L, (Supplementary Table 16). Specifically, BMDMs adhered to E-selectin and treated with LPS + VCR released approximately 2.5-fold more IL-10 (Fig. 5M) and 1.4-fold more IL-1β (Fig. 5N) compared to IgG2b controls. Notably, only IL-1β release, not of other cytokines, was significantly inhibited by pre-treatment with the NLRP3 inflammasome inhibitor MCC950 (5 μM), indicating a specific inflammasome-dependent mechanism (values of the cytokines in test and control conditions are shown in Supplementary Table 16).

E-selectin adhesion enhances NLRP3 signalling in vincristine-induced neuropathy

Given the established role of the NLRP3 inflammasome in vincristine-induced IL-1β release, we next investigated whether the effects of E-selectin on IL-1β release observed above in our study are specifically mediated through enhanced NLRP3 inflammasome activation. To assess this, we employed ASC-citrine reporter BMDMs, which allow real-time quantification of ASC speck formation (Figure 6A) - a direct readout of NLRP3 inflammasome activation.

BMDMs adhered to E-selectin and treated with lipopolysaccharide (LPS, 10 ng/mL) and vincristine (VCR, 100 μM) formed ASC specks more rapidly and in significantly greater numbers compared to cells adhered to IgG or P-selectin (Fig. 6B; Supplementary Table 17). A similar enhancement in ASC speck formation was observed when E-selectin–adhered BMDMs were treated with LPS (10 ng/mL) and nigericin (5 μM) (Fig. 6C; Supplementary Table 18). In both cases, ASC speck formation was completely abrogated by pre-treatment with MCC950 (10 μM), a selective NLRP3 inflammasome inhibitor, confirming that the observed effects were NLRP3-dependent (Fig. 6B; Supplementary Fig. S5A-B; Supplementary Table 17-18).

This increase in ASC speck formation was accompanied by significantly elevated secretion of IL-1β from E-selectin–adhered BMDMs in response to both LPS + VCR and LPS + nigericin (Fig. 6D; Supplementary Fig. S5C; Supplementary Table 19). By contrast, treatment with LPS, MCC950, nigericin, vincristine, or PBS alone, in the context of E-selectin adhesion, did not induce ASC speck formation (Supplementary Fig. S5; Supplementary Table 17-18) or IL-1β release (Supplementary Table 19).

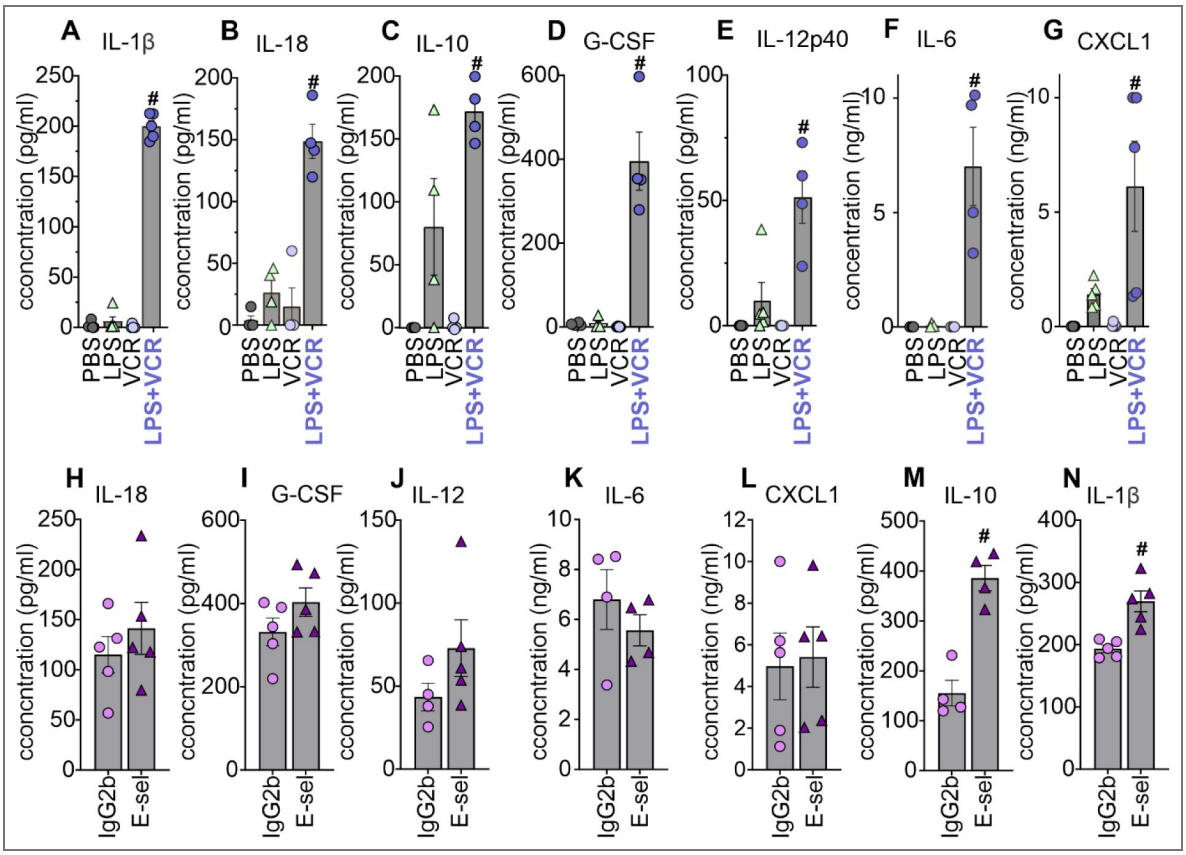

Fig. 5. E-selectin adhesion specifically enhances interleukin-1β release in vincristine-treated BMDMs.

(A-G) Release of IL-1β **(A)**, IL-18 **(B)**, IL-10 **(C)**, G-CSF **(D)**, IL12p40 **(E)**, IL-6 **(F)** and CXCL1 **(G)** is significantly higher in LPS-primed vincristine-treated (LPS+VCR) BMDMs compared to untreated (PBS), LPS-primed (LPS) or vincristine-treated (VCR) BMDMs. **(H-N)** Release of IL-18 **(H)**, G-CSF **(I)**, IL-12 **(J)**, IL-6 **(K)** and CXCL1 **(L)** is not different between BMDMs adhered to IgG2b (control) or E-sel (E-selectin). Release of IL-10 is ~2.5-fold higher **(M)** and release of IL-1β is ~1.4-fold higher **(N)** in BMDMs adhered to E-selectin. Statistical significance was determined using one-way ANOVA with Dunnett's multiple comparisons test, comparing LPS + VCR to LPS alone (A-G) or E-sel adhered to IgG2b adhered condition (n = 4 per group; #: $P < 0.05$).

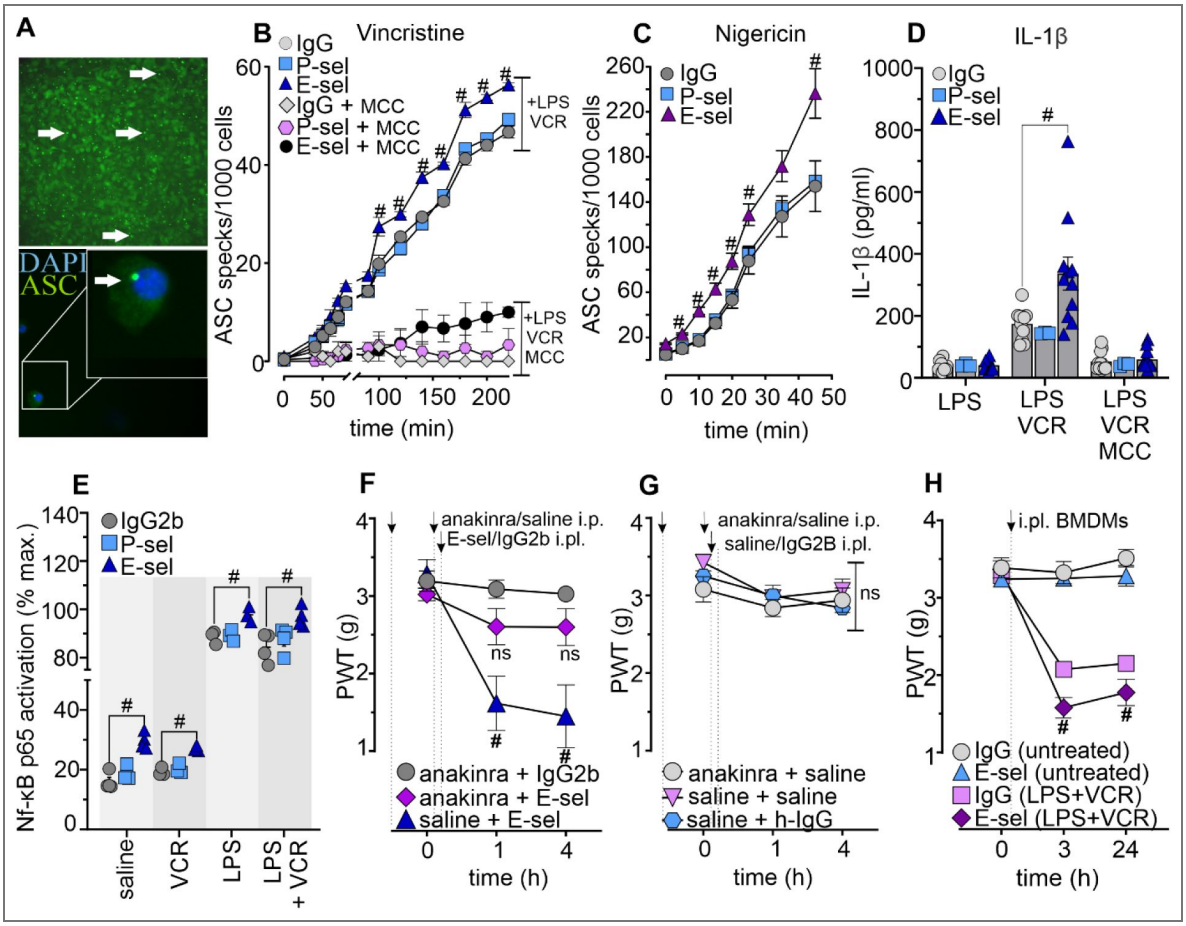

Figure 6. E-selectin functions as a non-canonical signalling amplifier of NF-κB–dependent NLRP3 activation and IL-1β release, driving vincristine-induced mechanical hypersensitivity.

(A) Representative images of ASC specks (green; white arrows) in bone marrow-derived macrophages (BMDMs) treated with lipopolysaccharide (LPS, 10 ng/mL) and vincristine (VCR, 100 μM). Nuclei are stained with DAPI (blue). Top: 10× magnification; bottom:60× magnification. **(B,C)** Quantification of ASC specks over time in ASC–citrine BMDMs adhered to E-selectin (E-sel), IgG2b, or P-selectin (P-sel) following treatment with LPS + VCR (B) or LPS + nigericin **(C)**. E-selectin adhesion significantly increased ASC speck formation compared to controls. This effect was fully blocked by pre-treatment with the NLRP3 inhibitor MCC950 (10 μM) and was mirrored by IL-1β release **(D)**. **(E)** Adhesion to E-selectin significantly increased the proportion of active p65 NF-κB across all treatment conditions (saline, vincristine, LPS, and LPS + vincristine) compared with IgG2b controls, whereas P-selectin did not induce comparable NF-κB activation. **(F)** Intraplantar (i.pl.) injection of E-selectin causes IL-1β-mediated mechanical hypersensitivity that is prevented by the IL-1 receptor antagonist anakinra (100 mg/kg; ip.). **(G)** Intraplantar administration of anakinra or saline prior to PBS or IgG2b i.pl. injection does not cause mechanical hypersensitivity. **(H)** Intraplantar injection of BMDMs treated with LPS + VCR and adhered to E-selectin induced significantly greater mechanical hypersensitivity compared to IgG2b-adhered controls. Injection of untreated BMDMs adhered to either E-sel or IgG2b had no effect. Statistical significance (#: $P < 0.05$) was determined using repeated measures two-way ANOVA (n = 6). Statistical significance (n=6) was determined by repeated-measures two-way **(C,F,G,H)** or one-way ANOVA **(D,E)** with Dunnett's multiple comparisons test (#$P < 0.05$).

To assess whether this response was specific to vincristine, BMDMs adhered to E-selectin, IgG, or PBS, were also treated with LPS in combination with other chemotherapeutic agents, including doxorubicin (DOX, 50 μM) and cyclophosphamide (CYC, 100 μM). Although low levels of IL-1β release were detected under these conditions, E-selectin adhesion had no significant effect, indicating that the potentiating effect of E-selectin is specific to vincristine (Supplementary Figure S5D-E, Supplementary Table 20).

Collectively, these data suggest that E-selectin does not simply function as a cellular adhesion molecule, but has additional, non-canonical functions as an amplifier of NLRP3 signalling and IL-1β release. Given that NF-κB signalling provides a critical priming step for NLRP3 activation, and that E-selectin engagement enhances NF-κB activity in leukocytes,[28] we hypothesised that E-selectin and vincristine pathways functionally converge on NF-κB to potentiate inflammasome activation and IL-1β release. Indeed, E-selectin adhesion significantly increased the proportion of active p65 NF-κB across all treatment conditions, compared to IgG2b controls (Fig. 6E).

Next, to determine whether these non-canonical signalling effects also contribute to development of vincristine-induced neuropathy *in vivo*, we assessed the effect of the IL-1 receptor antagonist anakinra on mechanical paw withdrawal thresholds following i.pl. injection of E-selectin (Fig. 6F-G). Interestingly, anakinra significantly attenuated E-selectin–induced mechanical hypersensitivity compared to saline (Fig. 6F, Supplementary Table 21), while no hypersensitivity was observed in control groups (Fig. 6G, Supplementary Table 21).

E-selectin-mediated enhancement of NLRP3-driven IL-1β release contributes to the development of VIPN in vivo

We previously demonstrated that intraplanar injection of BMDMs treated with LPS and vincristine into the hind paw of mice induces local mechanical allodynia resembling VIPN[8]. To assess whether the non-canonical signalling effects of E-selectin – leading to enhanced NLRP3 activation and IL-1β release in response to vincristine – also contribute to VIPN symptoms *in vivo*, we injected LPS + VCR–treated BMDMs adhered to E-selectin into the hind paw of mice. As expected, E-selectin–adhered BMDMs treated with LPS + VCR induced significantly more severe mechanical hypersensitivity than IgG2b-adhered cells (Fig. 6H). In contrast, intraplantar injection of untreated BMDMs adhered to either E-selectin or IgG2b had no effect on mechanical sensitivity.

Overall, our results position E-selectin as a putative anti-allodynic target for treatment of VIPN. We show that in addition to enhanced immune cell infiltration into neuronal tissue, immune cell adhesion to E-selectin directly enhances NLRP3-mediated IL-1β release via enhanced NfkB activation. We thus show a non-canonical signalling role of E-selectin in the pathogenesis of VIPN for the first time.

Discussion

Vincristine-induced peripheral neuropathy (VIPN) has traditionally been understood as a consequence of direct axonal toxicity and microtubule disruption. Our findings instead suggest a broader view: VIPN behaves as a neuroimmune network disorder in which interactions between adhesion molecules and immune cells reorganise communication within the dorsal root ganglia (DRG) before any clear structural nerve degeneration becomes apparent. Within this framework, E-selectin should not be considered simply as an adhesion molecule. Rather, it functions as a higher-level regulator that coordinates immune cell trafficking and amplifies inflammatory signalling within peripheral nerves.

By systematically examining multiple adhesion pathways, we identified a selective pathogenic signature in VIPN. Although both E-selectin and VCAM-1 contributed to vincristine-induced mechanical hypersensitivity and accumulation of F4/80$^+$ immune cells, blockade of ICAM-1, PECAM-1 or P-selectin did not provide protection (Fig. 1). This indicates that the neuropathy is not driven by broad endothelial activation, but instead depends on a specific adhesion axis. Importantly, the translational potential of targeting this axis differs between molecules. VCAM-1-directed therapies have encountered safety and implementation barriers, whereas E-selectin

inhibitors such as Uproleselan have already shown favourable tolerability in oncology trials [29–31]. This difference makes E-selectin a particularly actionable target within the vascular–immune interface.

Notably, persistent mechanical hypersensitivity occurred without loss of intraepidermal or myelinated nerve fibres (Fig. 2). This finding reframes VIPN in our model as a condition of functional neuroimmune reprogramming rather than primary structural degeneration. Spatial transcriptomic analyses revealed a consistent stress- and immune-associated transcriptional programme characterised by activation of mTORC1, engagement of unfolded protein response pathways, and induction of excitability-related genes including *Jun* and *Hcn2* (Fig. 3). These transcriptional changes did not occur in isolation. Instead, they were embedded within a reorganised intercellular communication landscape in which immune cells, fibroblasts, pericytes and Schwann cells acted as dominant signal senders across SPP1, Galectin, PTN, SEMA3 and growth factor pathways, while sensory neurons predominantly functioned as receivers. In this configuration, vincristine establishes a hierarchical inflammatory structure in which neuronal dysfunction is shaped by signalling from surrounding non-neuronal cells.

Importantly, perturbation of E-selectin did not eliminate this communication network but instead altered its structure (Fig. 3). The dominance of immune cells as signalling hubs was reduced, and stromal populations assumed greater mediator roles, without induction of *Sele* expression itself. These findings indicate that E-selectin does not simply act as a gene induced by vincristine; rather, it amplifies and stabilises inflammatory network states. In this sense, E-selectin may function as a regulatory gate that determines whether chemotherapeutic stress resolves adaptively or progresses into sustained nociceptive signalling.

Mechanistically, E-selectin exerts two converging effects. First, in its canonical role, it promotes F4/80$^+$ immune cell recruitment into neuronal tissues (Fig. 1), providing the cellular foundation for inflammation. Second, in a non-canonical role, it enhances NF-κB activation and NLRP3 inflammasome–dependent IL-1β release in macrophages, selectively amplifying cytokine production during vincristine exposure (Fig. 5-6). Together, these findings define a feed-forward inflammatory loop that operates upstream of neuronal sensitisation. Furthermore, intraplantar administration of E-selectin was sufficient to induce macrophage-dependent mechanical hypersensitivity *in vivo* via IL1R signalling, confirming that its pro-nociceptive effects arise primarily through immune–stromal interactions rather than direct neuronal activation (Fig. 4).

Collectively, these results support a model in which VIPN reflects dysregulated neuroimmune network dynamics rather than a simple linear axonopathy. Within this network, E-selectin occupies a central position, linking vascular adhesion to inflammasome activation and determining both the strength and persistence of pain signalling. Because E-selectin acts upstream of IL-1β and NLRP3, it represents a higher-order control point capable of influencing multiple downstream inflammatory pathways simultaneously.

This conceptual shift has clinical implications. VIPN remains a major reason for vincristine dose reduction or discontinuation, yet current treatment options are largely symptomatic. Duloxetine provides only modest benefit, and no established preventive therapies exist [32]. Targeting E-selectin offers a mechanistically grounded approach aimed at modifying disease progression rather than merely masking symptoms. The prior clinical development of E-selectin inhibitors enhances translational feasibility and raises the possibility of protecting neural function without compromising anti-tumour efficacy. Uproleselan (GMI-1271, small molecule E-selectin inhibitor) has been evaluated in multiple AML trials, including early phase I/II studies (NCT02306291, NCT03381795), a phase III trial in relapsed/refractory AML (NCT03616470), a phase III study in newly diagnosed older adults (NCT03701308), and additional combination studies in newly diagnosed AML (NCT04848974) showing generally favourable tumour adverse event profiles. Nevertheless, careful evaluation in human cohorts is required to determine whether targeting this vascular–immune axis can provide effective analgesia without impairing immune competence or chemotherapy effectiveness.

Several limitations should be considered. The study relies predominantly on murine models, which may not fully replicate the complexity and heterogeneity of VIPN in patients. Spatial transcriptomic analyses were performed on a limited number of biological replicates. Behavioural assessments focused mainly on mechanical hypersensitivity, and the diversity of tissue-resident macrophage populations was not directly characterised. In addition, the long-term systemic consequences of sustained E-selectin inhibition in tumour-bearing hosts remain unknown. Future studies should examine how this adhesion-dependent network evolves over time, whether similar mechanisms operate across different chemotherapeutic agents, and how cell-type–specific manipulation of E-selectin signalling reshapes nociceptive circuitry.

Conclusion

In conclusion, our findings show that E-selectin plays a central role in coordinating the immune and inflammatory processes that drive vincristine-induced peripheral neuropathy. Rather than simply treating symptoms, targeting E-selectin offers the possibility of intervening earlier in the disease process by disrupting the inflammatory pathways that sustain chemotherapy-induced neuropathy.

Supplementary figures

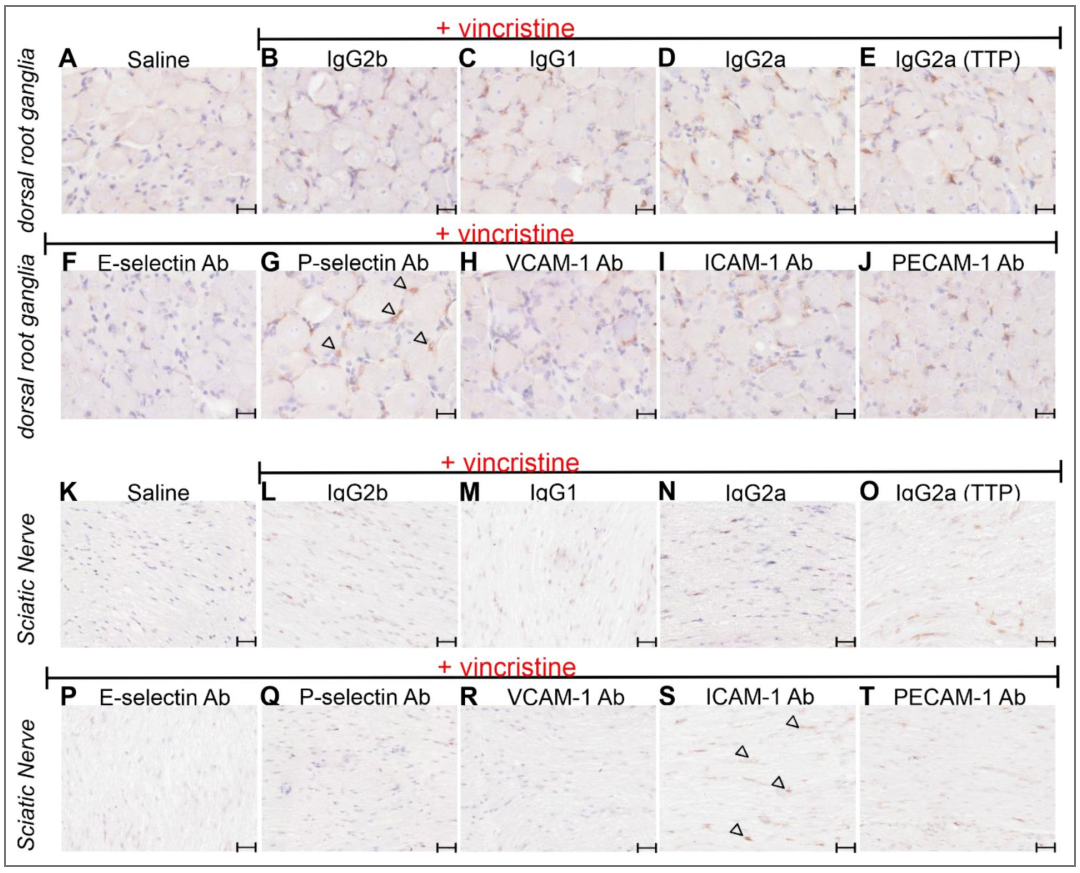

Supplementary Fig. S1. Representative immunohistochemical images of F4/80⁺ area in dorsal root ganglia and sciatic nerve 25 h post-vincristine administration. Mice received two intraperitoneal (i.p.) injections of antibodies targeting E-selectin (E-sel Ab), P-selectin (P-sel Ab), VCAM-1 (VCAM-1 Ab), ICAM-1 (ICAM-1 Ab), and PECAM-1 (PECAM-1 Ab), or corresponding isotype control antibodies (IgG2B, IgG1, IgG2A(TTP)) (10 mg/kg; i.p.) at two time points (t -24h, t -1h). This was followed by a single vincristine injection (0.5 mg/kg, i.p., time point t 0h). Shown are representative pictures of F4/80⁺ area in dorsal root ganglia **(A-J)** and sciatic nerve **(K-T)** in a saline control group **(A; K)** and following pretreatment with isotype control antibodies **(B-E; L-O)** or adhesion molecule-inhibiting antibodies **(F-J;P-T)**. Scale bar = 20 µm for DRGs or 10 µm for SN. Examples of F4/80⁺ area (brown stain) indicated by arrowheads.

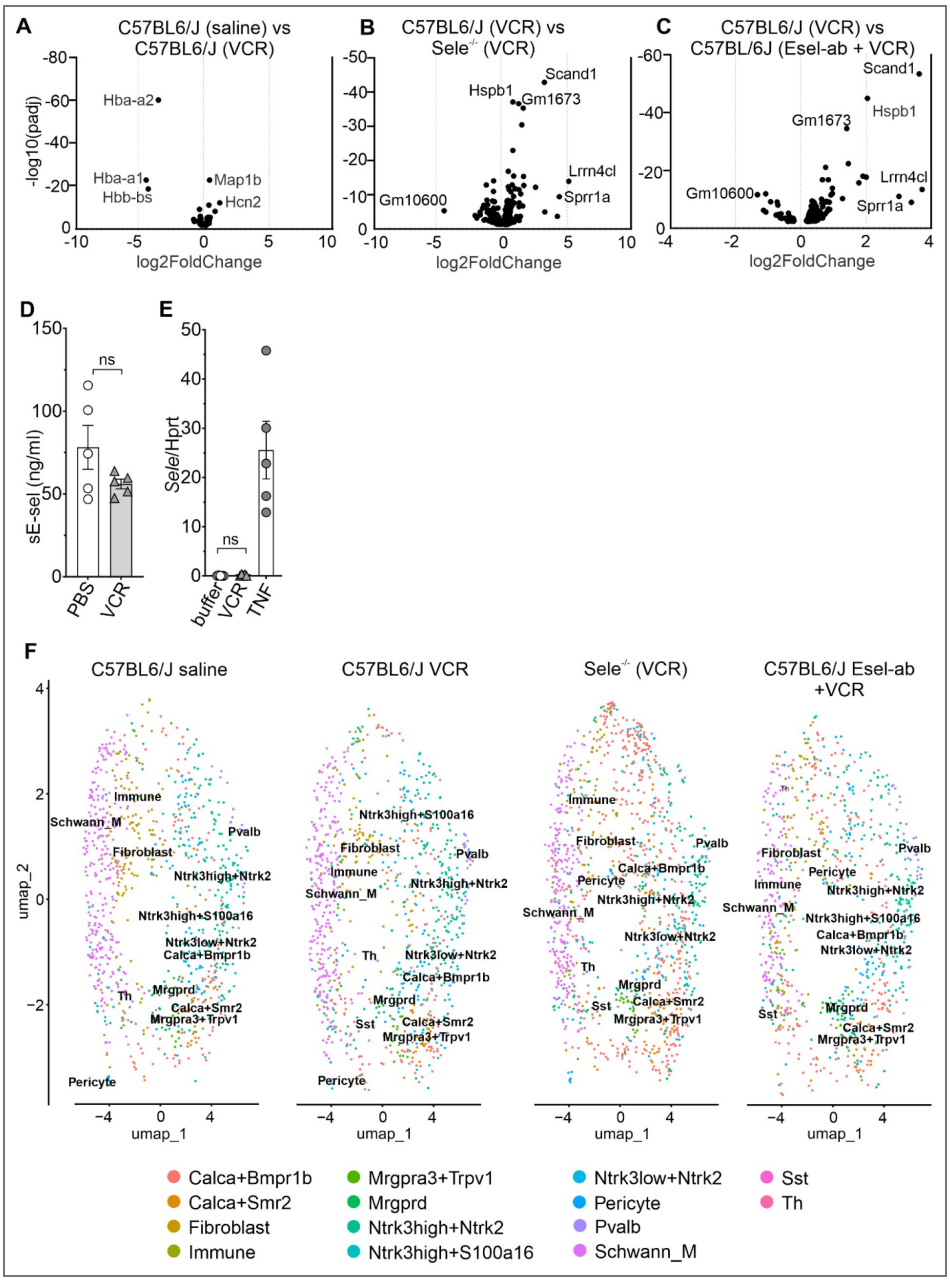

Supplementary Fig. S2. Vincristine induces a stress and injury transcriptional programme in dorsal root ganglia without upregulating E-selectin.

(A–C) Volcano plots of pseudobulk differential gene expression in dorsal root ganglia (DRG). **(A)** C57BL6/J saline versus vincristine (VCR) reveals induction of injury- and excitability-associated genes (e.g. Map1b, Hcn2) and downregulation of haemoglobin genes (Hba-a1, Hba-a2, Hbb-bs). **(B)** C57BL6/J (VCR) versus Sele^{-}/$^{-}$(VCR) and **(C)** C57BL6/J (VCR) versus C57BL6/J E-selectin antibody pre-treatment (Esel-ab + VCR) identify stress-related transcripts (e.g. Hspb1, Scand1) associated with E-selectin perturbation. **(D–E)** Circulating soluble E-selectin plasma protein levels in C57BL6/J mice treated with vincristine (0.5 mg.kg, i.p., once) and Sele transcript expression in HUVEC cells treated with vincristine for 24 hours, show no induction of Sele expression by vincristine, while Tnf serves as a positive control (ns, not significant). **(F)** UMAP projections of cell types across conditions (saline, VCR, Sele^{-}/$^{-}$ VCR, Esel-ab + VCR) demonstrate preservation of major neuronal and non-neuronal cell populations. Abbreviations: VCR: vincristine; Sele$^{-/-}$: E-selectin–deficient mice; Esel-ab: E-selectin–blocking antibody; DRG: dorsal root ganglion; TNF: tumour necrosis factor; Schwann_M: myelinating Schwann cells; Calca^{+}Bmpr1b and Calca^{+}Smr2: peptidergic sensory neuron subtypes; Mrgpra3^{+}Trpv1: nociceptive/pruriceptive neurons; Mrgprd: non-peptidergic sensory neurons; Ntrk3^high/+Ntrk2 and Ntrk3^low/+Ntrk2: sensory neuron subsets; Pvalb: parvalbumin-expressing interneurons; Sst: somatostatin-expressing neurons; Th: tyrosine hydroxylase–expressing neurons; Immune: aggregated immune cell populations; sE-sel: soluble E-selectin.

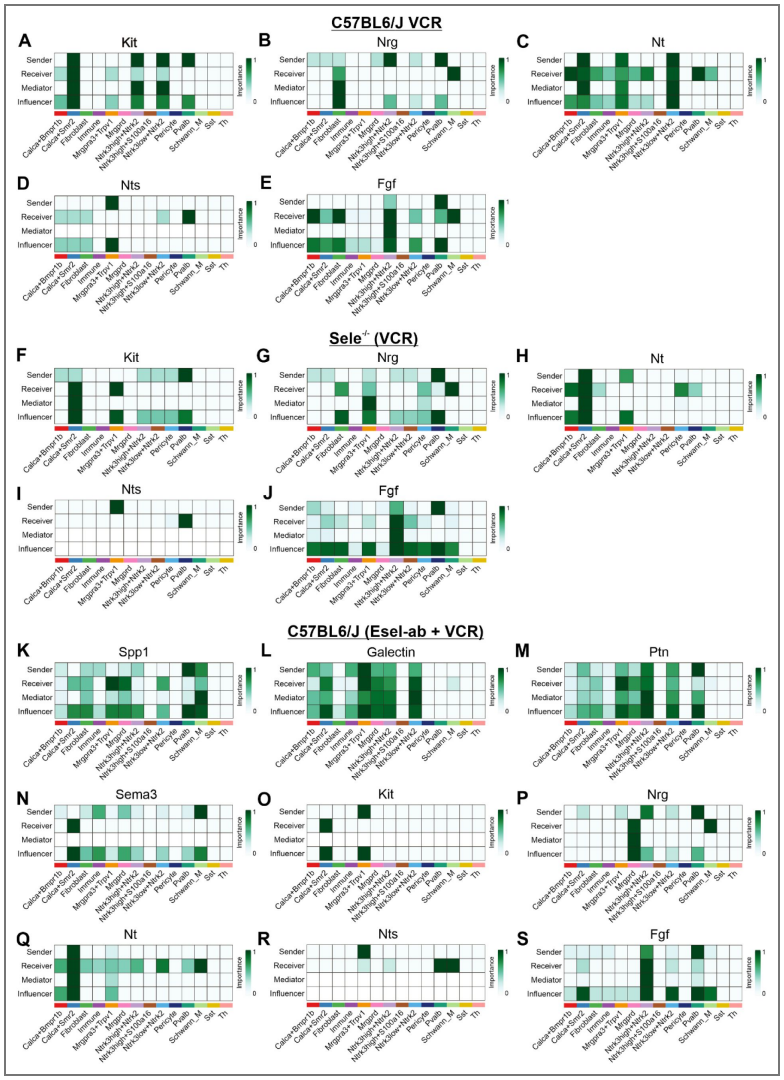

Supplementary Fig. S3. Vincristine and E-selectin perturbation reshape growth factor and neuromodulatory communication networks in dorsal root ganglia.

CellChat analysis was used to infer ligand–receptor–mediated communication networks in dorsal root ganglia (DRG) following vincristine treatment, highlighting pathway-specific sender, receiver, mediator and influencer roles across neuronal and non-neuronal cell populations. **(A–E)** Growth factor and neuromodulatory signalling pathways in C57BL6/J mice treated with vincristine (VCR). Heatmaps depict the relative contribution of each annotated cell type as senders, receivers, mediators or influencers for KIT (A), NRG (B), NT (C), NTS (D) and FGF (E) pathways, with darker green indicating higher importance scores. **(F–J)** Corresponding analyses in Sele^{-}/$^{-}$ mice treated with vincristine (VCR) show preservation of KIT, NRG, NT, NTS and FGF pathways but redistribution of communication roles across neuronal, glial and stromal populations. **(K–S)** Analyses in C57BL6/J mice treated with vincristine following E-selectin antibody pre-treatment (Esel-ab + VCR). Heatmaps illustrate altered sender, receiver, mediator and influencer contributions for SPP1 (K), GALECTIN (L), PTN (M), SEMA3 (N), KIT (O), NRG (P), NT (Q), NTS (R) and FGF (S) pathways, highlighting further redistribution of signalling roles relative to genetic E-selectin deletion. Across all panels, rows indicate inferred communication roles (sender, receiver, mediator, influencer) and columns represent annotated DRG cell populations; colour intensity reflects relative importance within each pathway. VCR: vincristine; Sele^{-}/$^{-}$: E-selectin–deficient mice; DRG: dorsal root ganglion; Schwann_M: myelinating Schwann cells; Calca^{+}Bmpr1b and Calca^{+}Smr2: peptidergic sensory neuron subtypes expressing Calca with Bmpr1b or Smr2, respectively; Mrgprd: non-peptidergic sensory neurons; Mrgpra3^{+}Trpv1: nociceptive/pruriceptive neurons; Ntrk3^high/+Ntrk2 and Ntrk3^low/+Ntrk2: sensory neuron subsets defined by relative Ntrk3 and Ntrk2 expression; Pvalb: parvalbumin-expressing interneurons; Sst: somatostatin-expressing neurons; Th: tyrosine hydroxylase–expressing neurons; Immune: aggregated immune cell populations; KIT: stem cell factor receptor signalling; NRG: neuregulin signalling; NT: neurotrophin signalling; NTS: neurotensin signalling; FGF: fibroblast growth factor signalling; SPP1: osteopontin signalling; PTN: pleiotrophin signalling; SEMA3: semaphorin 3 signalling.

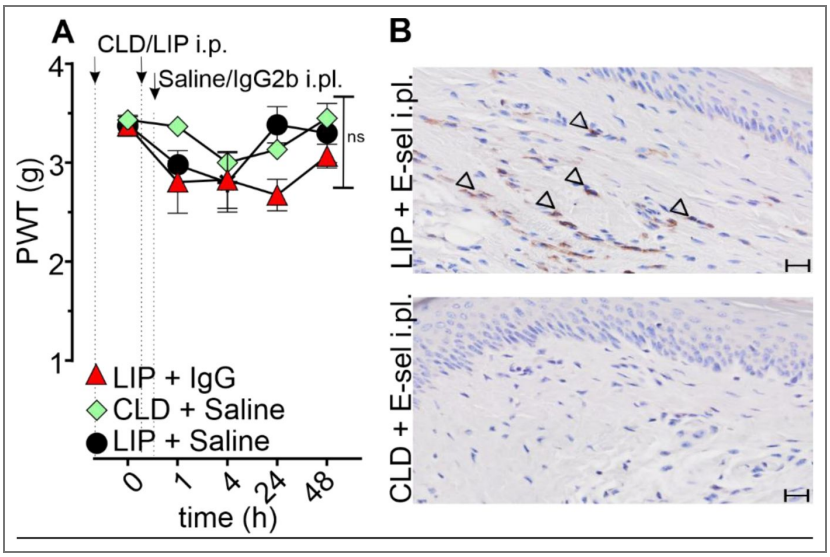

Supplementary Fig. S4.

(A) Control groups treated with liposomes (LIP), clodronate liposomes (CLD), saline or IgG2b did not develop mechanical hypersensitivity. **(B)** Representative images of F4/80⁺ immunohistochemistry in footpad skin of mice pretreated with CLD or LIP and injected with i.pl. E-selectin. Statistical significance (#: $P < 0.05$) was determined using repeated measures two-way ANOVA (n = 6-9).

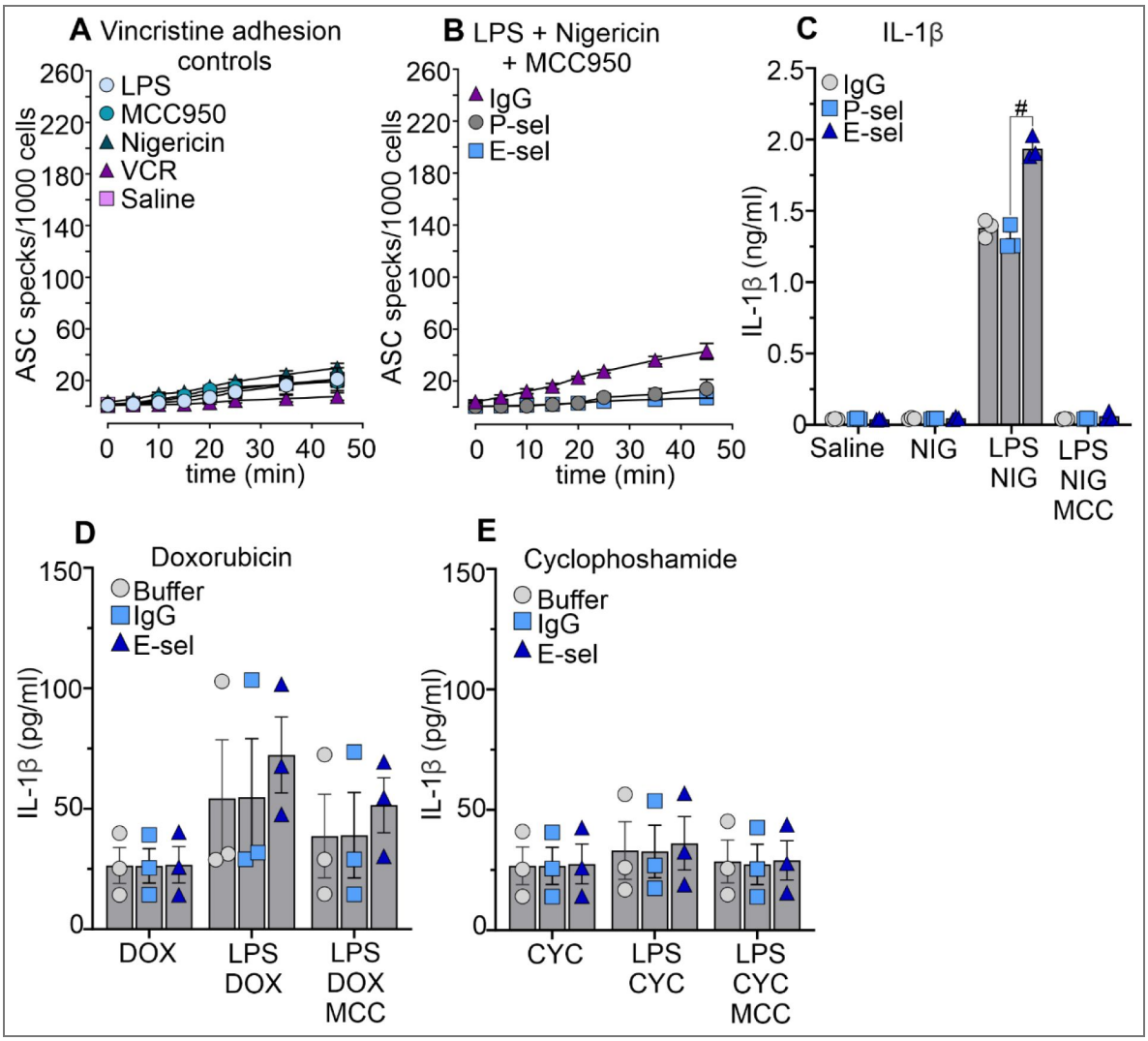

Supplementary Figure S5. E-selectin enhances ASC speck formation and IL-1β release in vincristine- or nigericin-treated BMDMs.

(A) No significant ASC speck formation was observed in E-selectin–adhered BMDMs treated with LPS, MCC950, nigericin, vincristine (VCR), or saline alone. (B,C) The NLRP3 inhibitor MCC950 (10 μM) prevents ASC speck formation **(B)** and IL-1β release **(C)** induced by treatment with lipopolysaccharide (LPS, 10ng/ml) + nigericin (5 μM). **(D–E)** IL-1β release from BMDMs treated with LPS + doxorubicin (DOX, 50 μM) (D) or LPS + cyclophosphamide (CYC, 100 μM) (E) adhered to E-sel, IgG2b, or P-sel. No significant differences were observed across conditions. Statistical analysis: two-way ANOVA **(A-B)**, one-way **(C,D,E)** (#P < 0.05); n≥3.

Data availability

RNAseq data will be uploaded at GEO upon acceptance of the manucript. All data generated or analyzed during this study are included in the manuscript and supporting files; source data files have been provided for all figures uppon reasonable request.

Acknowledgements

We thank the IMB Advanced Microscopy Facility (IMB AMF) and the IMB Sequencing facility for technical support. We thank Ms. Andree Axelsen and the NHMRC (1186835) for the financial support of this study. Starobova was supported by NHMRC Investigator grant 2024/GNT2034754; Tay was supported by the Childhood Cancer Research Scholarship and the E.M.A and M.C Henker Postgraduate Medical Research Scholarship, Alshammari was supported by the University of Hafr Al Batin, Saudi Arabia scholarship; Shatunova was supported by the University of Queensland International Scholarship and Mater Foundation; Vetter was supported by NHMRC Investigator grant 2017086. This work was also supported by the Kids' Cancer Project.

Additional information

Authors contributions

HS, IGW and IV conceived and supervised the study. HS and IV secured funding. HS, AA, NT, SS, AL, FI, VR-M, BH, SK and DLB performed experiments. HS, IV, QN, MMM, DTF and NNI performed data analysis, including spatial transcriptomic analyses. HS, LL, GC, CM, AR, AP, JLS, IGW and IV provided key reagents, materials and resources. HS and IV wrote the manuscript with input from all authors. All authors reviewed and approved the final manuscript.

Funding

Funder	Grant reference number	Author
DHAC | National Health and Medical Research Council (NHMRC)	2024/GNT2034754	Hana Starobova
DHAC | National Health and Medical Research Council (NHMRC)	2017086	Irina Vetter

Author ORCID iDs

Hana Starobova: https://orcid.org/0000-0001-9401-1744
Theodore Price: https://orcid.org/0000-0002-6971-6221
Irina Vetter: https://orcid.org/0000-0002-3594-9588

Additional files

Supplementary tables.

References

1 **Rowe JM,** et al. (2005) Induction therapy for adults with acute lymphoblastic leukemia: results of more than 1500 patients from the international ALL trial: MRC UKALL XII/ECOG E2993. *Blood* **106**:3760-3767 https://doi.org/10.1182/blood-2005-04-1623 | PubMed

2 **Bassan R,** Hoelzer D (2011) Modern therapy of acute lymphoblastic leukemia. *Journal of clinical oncology* **29**:532-543 https://doi.org/10.1200/jco.2010.30.1382 | PubMed

3 **O'Brien S,** et al. (2013) High-dose vincristine sulfate liposome injection for advanced, relapsed, and refractory adult Philadelphia chromosome–negative acute lymphoblastic leukemia. *Journal of Clinical Oncology* **31**:676-683 https://doi.org/10.1200/JCO.2012.46.2309 | PubMed

4 **Tay N,** et al. (2022) Chemotherapy-induced peripheral neuropathy in children and adolescent cancer patients. *Frontiers in molecular biosciences* **9** https://doi.org/10.3389/fmolb.2022.1015746 | PubMed

5 **Mora E,** Smith EML, Donohoe C, Hertz DL (2016) Vincristine-induced peripheral neuropathy in pediatric cancer patients. *American journal of cancer research* **6**:2416 PubMed

6 **Starobova H,** Vetter I (2017) Pathophysiology of chemotherapy-induced peripheral neuropathy. *Frontiers in molecular neuroscience* **10**:174 https://doi.org/10.3389/fnmol.2017.00174 | PubMed

7 **Old EA,** et al. (2014) Monocytes expressing CX3CR1 orchestrate the development of vincristine-induced pain. *J Clin Invest* **124**:2023-2036 https://doi.org/10.1172/JCI71389 | PubMed

8 **Starobova H,** et al. (2021) Vincristine-induced peripheral neuropathy is driven by canonical NLRP3 activation and IL-1β release. *Journal of Experimental Medicine* **218** https://doi.org/10.1084/jem.20201452 | PubMed

9 **Silva M,** Videira PA, Sackstein R (2018) E-selectin ligands in the human mononuclear phagocyte system: implications for infection, inflammation, and immunotherapy. *Frontiers in immunology* **8**:1878 https://doi.org/10.3389/fimmu.2017.01878 | PubMed

10 **Jia M,** et al. (2017) Activation of NLRP3 inflammasome in peripheral nerve contributes to paclitaxel-induced neuropathic pain. *Molecular pain* **13**:1744806917719804 https://doi.org/10.1177/1744806917719804 | PubMed

11 **Khan N,** Kuo A, Brockman DA, Cooper MA, Smith MT (2018) Pharmacological inhibition of the NLRP3 inflammasome as a potential target for multiple sclerosis induced central neuropathic pain. *Inflammopharmacology* **26**:77-86 https://doi.org/10.1007/s10787-017-0401-9 | PubMed

12 **Binshtok AM,** et al. (2008) Nociceptors are interleukin-1β sensors. *Journal of Neuroscience* **28**:14062-14073 https://doi.org/10.1523/jneurosci.3795-08.2008 | PubMed

13 **Starobova H,** et al. (2025) Inhibition of the NLRP3 inflammasome using MCC950 reduces vincristine-induced adverse effects in an acute lymphoblastic leukemia patient-derived xenograft model. *Hemasphere* **9**:e70092 https://doi.org/10.1002/hem3.70092 | PubMed

14 **Bierschenk D,** et al. (2019) The Salmonella pathogenicity island-2 subverts human NLRP3 and NLRC4 inflammasome responses. *Journal of leukocyte biology* **105**:401-410 https://doi.org/10.1002/jlb.ma0318-112rr | PubMed

15 **Schroder K,** et al. (2012) Conservation and divergence in Toll-like receptor 4-regulated gene expression in primary human versus mouse macrophages. *Proceedings of the National Academy of Sciences* **109**:E944-E953 https://doi.org/10.1073/pnas.1110156109 | PubMed

16 **Coll RC,** et al. (2019) MCC950 directly targets the NLRP3 ATP-hydrolysis motif for inflammasome inhibition. *Nature chemical biology* **15**:556-559 https://doi.org/10.1038/s41589-019-0277-7 | PubMed

17 **Han C,** et al. (2018) The Novel Activity of Carbamazepine as an Activation Modulator Extends from Na(V)1.7 Mutations to the Na(V)1.8-S242T Mutant Channel from a Patient with Painful Diabetic Neuropathy. *Mol Pharmacol* **94**:1256-1269 https://doi.org/10.1124/mol.118.113076 | PubMed

18 **Gilding EK,** et al. (2020) Neurotoxic peptides from the venom of the giant Australian stinging tree. *Sci Adv* **6** https://doi.org/10.1126/sciadv.abb8828 | PubMed

19 **Tay N,** et al. (2025) A comprehensive protocol for simplified mouse DRG fixation, processing and F4/80 immunohistochemistry: Overcoming common challenges. *J Neurosci Methods* **418**:110434 https://doi.org/10.1016/j.jneumeth.2025.110434 | PubMed

20 **Starobova H,** et al. (2019) Minocycline Prevents the Development of Mechanical Allodynia in Mouse Models of Vincristine-Induced Peripheral Neuropathy. *Front Neurosci* **13**:653 https://doi.org/10.3389/fnins.2019.00653 | PubMed

21 **Deuis JR,** Vetter I (2016) The thermal probe test: A novel behavioral assay to quantify thermal paw withdrawal thresholds in mice. *Temperature (Austin)* **3**:199-207 https://doi.org/10.1080/23328940.2016.1157668 | PubMed

22 **Starobova H,** et al. (2021) Vincristine-induced peripheral neuropathy is driven by canonical NLRP3 activation and IL-1beta release. *J Exp Med* **218** https://doi.org/10.1084/jem.20201452 | PubMed

23 **Cavaletti G,** et al. (1992) Morphometric study of the sensory neuron and peripheral nerve changes induced by chronic cisplatin (DDP) administration in rats. *Acta Neuropathol* **84**:364-371 https://doi.org/10.1007/BF00227662 | PubMed

24 **Ballarini E,** et al. (2022) Sodium-Calcium Exchanger 2: A Pivotal Role in Oxaliplatin Induced Peripheral Neurotoxicity and Axonal Damage?. *Int J Mol Sci* **23** https://doi.org/10.3390/ijms231710063 | PubMed

25 **Montague K,** Simeoli R, Valente J, Malcangio M (2018) A novel interaction between CX3CR1 and CCR2 signalling in monocytes constitutes an underlying mechanism for persistent vincristine-induced pain. *Journal of neuroinflammation* **15**:1-15 https://doi.org/10.1186/s12974-018-1116-6 | PubMed

26 **Starobova H,** Mueller A, Deuis JR, Carter DA, Vetter I (2020) Inflammatory and neuropathic gene expression signatures of chemotherapy-induced neuropathy induced by vincristine, cisplatin, and oxaliplatin in C57BL/6J mice. *The journal of pain* **21**:182-194 https://doi.org/10.1016/j.jpain.2019.06.008 | PubMed

27 **Jain A,** et al. (2024) Nociceptor-immune interactomes reveal insult-specific immune signatures of pain. *Nature Immunology* **25**:1296-1305 https://doi.org/10.1038/s41590-024-01857-2 | PubMed

28 **Davies JM,** Radford KJ, Begun J, Levesque JP, Winkler IG (2021) Adhesion to E-selectin primes macrophages for activation through AKT and mTOR. *Immunology and Cell Biology* **99**:622-639 https://doi.org/10.1111/imcb.12447 | PubMed

29 **O'Connor P,** et al. (2005) Relapse rates and enhancing lesions in a phase II trial of natalizumab in multiple sclerosis. *Multiple Sclerosis Journal* **11**:568-572 https://doi.org/10.1191/1352458505ms1205oa

30 **Shirani A,** Stüve O (2018) Natalizumab: perspectives from the bench to bedside. *Cold Spring Harbor Perspectives in Medicine* **8**:a029066 https://doi.org/10.1101/cshperspect.a029066 | PubMed

31 **Pickett JR,** Wu Y, Zacchi LF, Ta HT (2023) Targeting endothelial vascular cell adhesion molecule-1 in atherosclerosis: drug discovery and development of vascular cell adhesion molecule-1-directed novel therapeutics. *Cardiovasc Res* **119**:2278-2293 https://doi.org/10.1093/cvr/cvad130 | PubMed

32 **Chow R,** et al. (2023) Duloxetine for prevention and treatment of chemotherapy-induced peripheral neuropathy (CIPN): systematic review and meta-analysis. *BMJ Support Palliat Care* **13**:27-34 https://doi.org/10.1136/spcare-2022-003815 | PubMed

Peer reviews

Reviewer #1 (Public review):

This paper looks at the effect of vincristine-induced peripheral neuropathy (VIND), a common effect of cancer therapy. The authors performed in vivo experiments in mice by injecting them with vincristine sulphate i.p. (+/- various inhibitors or antibodies) or E-selectin intraplantar (*i.pl*.), and in vitro experiments using dorsal root ganglia (DRG) neurons and bone marrow derived macrophages (BMDMs).

Inhibition of E-selectin with antibodies or genetic depletion reduced the accumulation of F4/80+ macrophages in the DRG and sciatic nerves (located beside the spine) after vincristine administration, and attenuated the mechanical hypersensitivity (paw withdrawal).

The authors went on to perform spatial transcriptomics on isolated DRG neurons and found some pathways changed. E-selectin injected directly intraplantar (*i.pl*.) mimicked the effect of vincristine administration on the mechanical hypersensitivity. Whereas chlodronate depletion of myeloid cells reduced these changes in the E-selectin model. Using LPS priming before vincristine in BMDMs in vitro, the authors demonstrate an increase in many cytokines, including IL-1beta (typically associated with the formation of an inflammasome) and elevated p-NFkB. Finally, treatment of mice with anakinra (which neutralizes IL-1beta)

also attenuated the E-selection-induced reduction in mechanical hypersensitivity when injected *i.pl*.

The authors address an important aspect that after cancer therapy, there can be peripheral nerve damage that has lasting consequences for patients, although the precise mechanism is unknown. The authors delineate that E-selectin has an important role in the mouse model, where depletion or inhibition attenuated the negative effect of vincristine (i.p.) on mechanical hypersensitivity (paw withdrawal). Administration of E-selectin into the foot (*i.pl*.) also mimicked the changes observed in the vincristine-treated mice. There seems to be a role for macrophages, as they were associated with DRGs in vivo, and depletion attenuated motor deficits in the E-selectin injection model.

However, I am not convinced by the data supporting some of the conclusions drawn by the authors, particularly on the role of the NLRP3 inflammasome in their in vivo model.

Main points:

(1) The initial experimental paradigm looks at the DRG neurons, which are located by the spine, and from there the foot pad is examined in subsequent experiments. It would be relevant to show whether the foot pad is altered in the vincristine-treated mice and whether the infiltration of myeloid cells that was demonstrated at DRGs is also observed in the foot in the vincristine model. Otherwise, the mechanism being investigated in the vincristine model, which might have similar functional results (paw withdrawal), but the mechanism behind both could be completely different.

(2) The rationale of performing spatial sequencing on DRG neurons isolated from vincristine mice is unclear. It is likely that more information could have been obtained from looking at sections from these animals, and there would be a better link to the experiments on BMDMs which follow afterwards. Indeed, the spatial data does not seem to play a key role in the study. There is not a clear link between it (which was carried out on DRGs) and the later focus on macrophages and indeed the NLRP3 inflammasome.

(3) The authors suggest that the E-selectin is enhancing NFkB-induced priming of the NLRP3 inflammasome. LPS+vincristine increased IL-1b release from BMDMs in vitro, which was elevated in the presence of E-selectin. E-selectin also increased ASC speck formation by approx. 20% in vitro. The ASC speck formation in vitro was blocked by MCC950, a specific NLRP3 inhibitor, but the authors went on to use anakinra in vivo using the E-selectin *i.pl*. model. It is really unclear why the switch to anakinra occurred for the in vivo work, as blocking IL-1b is central to many inflammatory pathways, not just NLRP3. Use of MCC950 would have been more appropriate to demonstrate that negative effects on mechanical function are mediated by the NLRP3 inflammasome. As there were no readouts of NLRP3 inflammasome activity measured in any of the mice in vivo (e.g. local ASC specks, IL-1b release, western blot of typical inflammasome components such as IL-1b, caspase-1, ASC or gasdermin D) either at the DRG site or the foot, we cannot say that the cell culture data mimics or models the in vivo conditions at this time.

(4) Additionally, the reliance on the E-selectin administration models for the second half of the paper is curious. It would have been relevant to test whether the immune-modulating inhibitors could also attenuate the vincristine-induced effects on mechanism hypersensitivity, to better link the E-selectin model with the vincristine one.

(5) Details are missing from the figure legends and the methods. The concentrations of compounds used in cell culture and exposure times are not clear.

https://doi.org/10.7554/eLife.111950.1.sa1

Reviewer #2 (Public review):

Summary:

Using antibody treatments, genetic models and in vitro studies, the authors convincingly show that E-Selectin is a driver of VIPN.

Strengths:

In vivo studies are robust. Antibody studies as well as the inflammasome-related work are very well done.

Weaknesses:

(1) The spatial transcriptomics data need to be improved in terms of visualization.

The authors should plot genes that define the cell types in the sequencing dataset, and also show the cellular map on the cut, not only UMAPs. Can the authors not use the n=3 samples per condition to perform some statistical analyses? While the CellChat analyses are informative, they are difficult to read. Fold change over control when comparing conditions and pathways may be a better way of visualization.

(2) In Figure 1B, the % DAB is not easy to understand. It would be better to do the staining also via IF, and then maybe to count nuclei. The corresponding figures shown in the supplemental figure are not convincing. If F4/80 is not working well, Iba1 could be an alternative.

(3) The authors should define the background of all the mice used. Have they been back-crossed to B6j mice? One cannot compare C57BL6J mice with full knockouts if they are not littermate controls. Especially immunological responses are completely dependent on the background of mice. See e.g. PMID: 40568896.

(4) Could the authors comment on the role of ICAM2? Why was this not tested as well?

https://doi.org/10.7554/eLife.111950.1.sa0